Cropland and Population Exposure to Extreme Precipitation Events in Central Asia Under Future Climate Change

Tao Li[1,2], Jiayu Bao[3], Ye Yuan[1], Jinyu Chen[4], Fengjiao Song[1,2], Xiaoran Huang [1,2], Tao Yu[1,2], Gang Long[1,2], Jingyu Jin[1,2], Diwen Dong[1,2], Naibi Sulei [1,2], Ting Wang [1,2], and Anming Bao[1,5,6,7*]

[1] State Key Laboratory of Desert and Oasis Ecology, Key Laboratory of Ecological Safety and Sustainable Development in Arid Lands，Xinjiang Institute of Ecology and Geography, Chinese Academy of Sciences, Urumqi 830011, China

[2] University of Chinese Academy of Sciences, Beijing 100049, China

[3] Kunming University of Science and Technology, Yunnan Province, Kunming 650093, China

[4] Dongtai Agricultural Technology Extension Center, Jiangsu Province, Dongtai 224200, China

[5] China-Pakistan Joint Research Center on Earth Sciences, CAS-HEC, Islamabad, 45320, Pakistan

[6] Key Laboratory of GIS & RS Application Xinjiang Uygur Autonomous Region, Urumqi 830011, China

[7] Qinghai Forestry Carbon Sequestration Service Center, Xining 810001, China

*Corresponding Author: Anming Bao. E-mail: baoam@ms.xjb.ac.cn

Abstract: Central Asia (CA) is experiencing rapid warming, leading to more Extreme precipitation events (EPEs). However, the anticipated changes in cropland and population exposure to EPEs are still unexplored. In this study, projected changes in EPEs characteristics, as well as cropland and population exposure from EPEs are quantified using global climate model simulations. Our findings reveal a significant increase in the exposure of cropland and population to extreme precipitation over time. Specifically, under the high-emission SSP5-8.5 future pathway, the amount, frequency, intensity, and spatial extent of extreme precipitation in CA are projected to considerably amplify, particularly in the high mountain regions. Under the SSP5-8.5 scenario, cropland exposure in CA increases by 46.4%, with a total cropland exposure of approximately 190.7 million km² expected between 2021 and 2100. Additionally, under the SSP3-7.0 scenario, population exposure in CA increases by 92.6%, resulting in a total population exposure of about 48.1 billion person-days during the same period. The future maximum centers of exposure are concentrated over northern Kazakhstan and the tri-border region of Tajikistan, Kyrgyzstan, and Uzbekistan. Notably, the climate effect is more dominant than the other effects, whereas changes in population effect contribute to the total change in population exposure. Given the heterogeneous distribution of population and cropland in CA, it is imperative for the countries in the region to implement effective measures that harness extreme precipitation and cope with the impacts of these extreme climate events.

Keywords:
Extreme precipitation events; Cropland and Population Exposure; Central Asia; ISI-MIP3b

Key Points:

- Extreme precipitation events are projected to increase substantially over the 21st century in the mountainous regions across Central Asia.
- This study considers both population and cropland as vulnerable hazard-bearers to extreme precipitation in the exposure assessment.
- The population exposure is greatest in the SSP3-7.0 scenario and the cropland exposure is greatest in the SSP5-8.5 scenario.

Plain Language Summary: Climate change is anticipated to intensify the risk of extreme precipitation events (EPEs). When evaluating these risks, it is crucial to consider socioeconomic factors. This study employs projections based on five Global Climate Models (GCMs) to assess the socioeconomic impacts of precipitation extremes on cropland and population under three Representative Concentration Pathways (RCPs) and Shared Socioeconomic Pathways (SSPs) across four future time periods (2021-2040, 2041-2060, 2061-2080, and 2081-2100). The findings reveal a substantial increase in the exposure of the population and cropland in CA to extreme precipitation over time. Among the scenarios examined, the SSP3-7.0 scenario exhibits the highest population exposure, while the SSP5-8.5 scenario results in the highest cropland exposure in CA. It can be inferred that the climate influence is more dominant than the population and cropland, particularly for CA. Consequently, CA demands heightened attention due to the vulnerability of its population and cropland to EPEs. Moreover, CA must prioritize the implementation of effective adaptation measures due to its highly heterogeneous spatial distribution of population. Additionally, as a predominantly agricultural region with a significant reliance on water resources, the region faces exceptional challenges.

1. Introduction

In the context of global climate change, increasing evidence supports that climate change is responsible for triggering numerous extreme weather and climate events on a global scale (IPCC, 2021). Climate change is anticipated to accelerate the global hydrological cycle and intensify all forms of extreme weather and climate events (Ombadi et al., 2023; Zscheischler et al., 2020; Tabari et al., 2020; Zhou et al., 2023; Jong et al., 2023). EPEs are projected to become more intense, longer in duration, and more frequent (Jong et al., 2023; Huang et al., 2022; Zhang et al., 2021; Zhang et al., 2020), particularly in arid regions (Yao et al., 2021). Given the recent increase in the frequency and substantial impact of EPEs, they have garnered greater attention than ever before. To effectively prioritize research efforts and inform strategies for risk management, it is crucial to assess future risks, specifically examining the exposure of populations to specific hazards. However, it should be noted that such risks may vary by age, season, and geographical region (Samir et al., 2017).

EPEs led to significant consequences for substantial socioeconomic and ecological losses (Doan et al., 2022; Gao et al., 2020) also profound implications for human safety and property protection (Swain et al., 2020; Tandon et al., 2018). For instance, the extreme precipitation in China in 2010 resulted in thousands of deaths and extensive property damage due to landslides and mudslides (Wang et al., 2016). Similarly, extreme precipitation in northern Pakistan in 2010 claimed approximately 3,000 lives (Lau et al., 2012), while northern India experienced more than 5,000 casualties from EPEs in 2013 (Cho et al., 2016). EPEs have also been identified as a major contributor to crop yield reductions, surpassing the impacts of other extreme climate hazards (Fu et al., 2023; Hasegawa et al., 2021; Li et al., 2019; Basile et al., 2022). With further climate warming, these EPEs and associated hazards are expected to become more frequent across various regions of the world (Jiang et al., 2016; Cook et al., 2020). EPEs deserve more attention in arid and semi-arid regions. This is because arid and semi-arid regions are particularly prone to flooding, mudslides and landslides when extreme precipitation occurs (Mariotti et al., 2002; Xue et al., 2017; Xu et al., 2015; Zhang et al., 2017; Swain et al., 2015; Donat et al., 2016). Additionally, crops in arid regions are less resistant to extreme precipitation due to fragile ecosystems.

Central Asia (CA), a typical arid and semi-arid region, identified as a hotspot of global warming, is experiencing a temperature increase that is approximately twice as rapid as the global average (Zhang et al., 2019), and the warming trend is projected to persist throughout the 21st century (Huang et al., 2014; Guo et al., 2021). While some studies suggest a significant increase in mean precipitation and interannual variability across most of CA under future scenarios (Jiang et al., 2020; Zhao et al., 2018), the trend towards greater precipitation appears more prominent during the winter season (Yu et al., 2018). Additionally, the intensity of EPEs in CA is predicted to escalate in response to global warming (Peng et al., 2020). However, alternative models propose a potential trend towards drier summers, and projections for future drought exhibit higher uncertainty among models compared to changes in extreme precipitation (Jiang et al., 2020). The vulnerable ecosystems of CA, characterized by relatively sparse vegetation cover, are particularly susceptible to the impacts of global climate change (Hu et al., 2016; Yuan et al., 2017). CA is considered ecologically fragile, with changes in precipitation significantly influencing human production and livelihoods (Wei et al., 2023). Adverse climate events like floods have had detrimental effects on the region's delicate ecosystems, impeding socioeconomic and sustainable development (Dike et al., 2022; Scussolini et al., 2016). Given the limited resilience and adaptive capacity of the region, extreme climate change poses a significant challenge to livelihoods, exerting far-reaching impacts on various key socioeconomic sectors (Devkota et al., 2013; Liu et al., 2023). Furthermore, the economies of CA countries heavily rely on primary industries, particularly agriculture, which is highly vulnerable to changes in the local hydrological cycle (Gessner et al., 2013; Jiang et al., 2023). Modifications in precipitation patterns strongly impact the livelihoods of CA populations and the fragility of the environment. Moreover, both the population and cropland in CA are concentrated in areas prone to high flood risk, amplifying the risks associated with EPEs (Li et al., 2019). Addressing the adverse impacts of future EPEs in these vulnerable areas and quantifying the associated socioeconomic risks are imperative for policymakers and the development of climate adaptation strategies.

Recent studies indicate that global exposure to extreme precipitation is expected to increase in the future (Li et al., 2019; Shi et al., 2021). However, there have been relatively few long-term studies examining trends in EPEs. Furthermore, previous research on extreme precipitation in CA has primarily focused on historical and future analyses of spatial and temporal evolution, as well as attribution mechanisms (Ma et al., 2021; Zhang et al., 2021; Li et al., 2022; Jiang et al., 2021; Xu et al., 2022; Liu et al., 2022). Few studies have investigated the demographic and socioeconomic impacts of extreme precipitation in CA. As a result, there is a need to quantify future changes in extreme precipitation in the region and comprehensively assess the implications of heightened EPEs. Therefore, accurate prediction of changes in the characteristics of extreme precipitation under different future climate scenarios in CA is crucial for developing effective adaptation strategies in different regions to mitigate the risks posed by extreme precipitation.

This study aimed to examine future changes in extreme precipitation and the resulting exposure of population and cropland in CA using multi-model projections from the ISI-MIP framework. In comparison to CMIP5 and CMIP6, the ISI-MIP framework employs a novel, more federated approach that utilizes the 1960-1999 WATCH in-analysis data to downscale and bias correct climate model outputs. Furthermore, the ISI-MIP models generally operate at finer resolutions and adhere to a standardized modeling protocol, enhancing their ability to simulate climate extremes (Gao et al., 2020; Hempel et al., 2013; Warszawski et al., 2014; Yang et al., 2020). In this research, we specifically quantify the shifts in exposure to extreme precipitation under future warming scenarios. Given Central Asia's high population density and heavy reliance on agriculture, we focus on population and cropland as primary factors influencing exposure. The findings from this investigation are crucial for understanding the region's future vulnerability and for informing effective mitigation and adaptation strategies. Importantly, this study represents an early attempt to comprehensively and quantitatively evaluate the impact of future changes in extreme precipitation on Central Asia's population and cropland.

2. Study Area, Data and Methods

2.1 Study Area

The CA, comprises five countries that emerged following the dissolution of the Soviet Union: Kazakhstan, Uzbekistan, Kyrgyzstan, Tajikistan, and Turkmenistan (Figure 1). Situated in the heartland of the Eurasian continent, CA exhibits a diverse topography, with elevated terrain in the east and lower elevations in the west. CA is one of the largest arid and semi-arid regions within the mid-latitudes, and its intricate topography constitutes a primary driver of precipitation variability in the area (Schiemann et al., 2008; Murnane et al., 2017). The Himalayas, the Pamir Plateau, and the Hindu Kush act as barriers, shielding the region from the influence of moist air masses originating from the Indian Ocean. Consequently, air currents from the west predominantly shape the precipitation patterns in CA, with precipitation primarily occurring on the western slopes of the mountains (Xie et al., 2021; Li et al., 2021; Zou et al., 2021). The distribution of population in the region exhibits significant heterogeneity, with a high concentration observed in the tri-border area of Uzbekistan, Tajikistan, and Kyrgyzstan. Uzbekistan stands as the most populous country in CA, boasting a population

density of 70 persons/km², while Tajikistan follows closely behind with a population density second only to Uzbekistan (61 persons/km²). Notably, Tajikistan's population density is ten times higher than that of Kazakhstan, which holds the largest land area among the CA countries. All five countries in CA heavily rely on agriculture, with the sector employing over 50% of the workforce and contributing to approximately one-fifth of the total GDP. Cotton and wheat serve as the primary crops in the region, emphasizing the paramount role of agriculture in Central Asia's economic landscape (Hamidov et al., 2016; Sommer et al., 2013). Over the past three decades, the region has witnessed a rapid increase in temperature, surpassing the warming rates observed in neighboring areas and the global average (Gong et al., 2017).

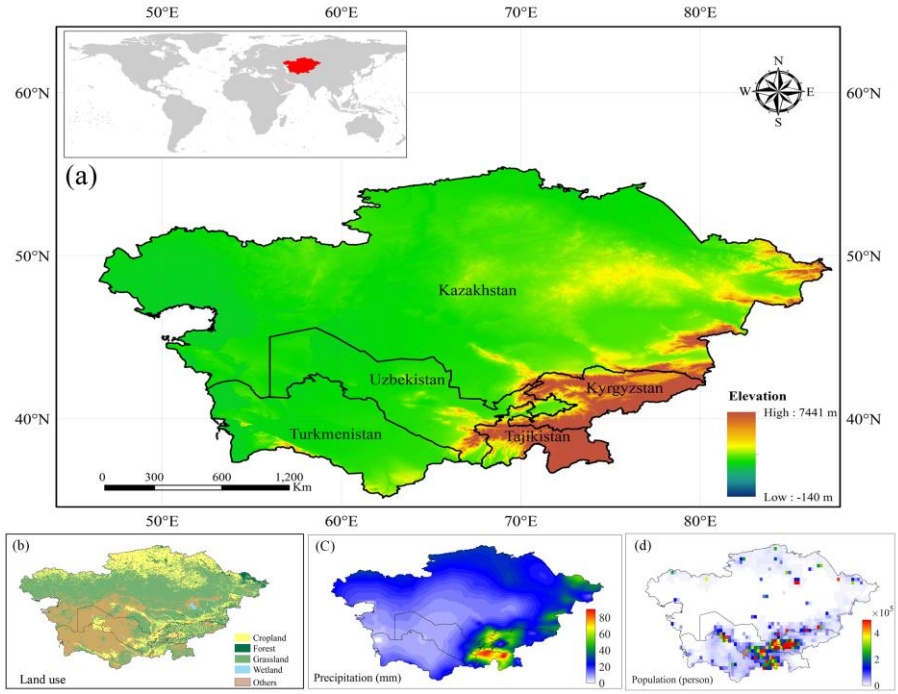

Figure 1. Map of study area. (a) Location and topography in Central Asia. (b) Land use types in Central Asia. (c) Mean monthly precipitation from1995 to 2014. (d) Spatial distribution of population in 2020 under SSP1-2.6 scenario simulated by the model.

2.2 Dataset

Gridded precipitation products are extensively utilized for the assessment of climate model data. In this study, monthly precipitation data at a spatial resolution of 0.5° is obtained from the latest Climate Research Unit dataset (CRU TS 4.07). This dataset is based on data collected from over 4,000 weather stations worldwide and is widely recognized as one of the most prominent climate datasets available. The dataset, produced by the National Centre for Atmospheric Sciences (NCAS) in the U.K, provides monthly-scale data covering the land surface from 1901 to 2022 (Harris et al., 2020; Liu et al., 2021). The CRU dataset has been extensively employed for various applications, including the identification of extreme precipitation, analysis of extreme weather climates, and bias correction for General Circulation Model (GCM) simulations (Zhang et al., 2022; Hao et al., 2018). For the purpose of this study, monthly precipitation data from CRU was used to evaluate the data obtained from the selected GCMs and perform necessary corrections.

The 5 GCMs (Table 1) including GFDL-ESM4, IPSL-CM6A-LR, MPI-ESM1-2-HR, MRI-ESM2-0, and UKESM1-0-LL were utilized in this study. These GCMs were provided by the Intersectoral Impact Model Intercomparison Project (ISI-MIP). These 5 models were selected based on their availability of daily data for the historical period from 1950 to 2100, covering all future scenarios and variables required for analysis. Additionally, all five models are part of both the CMIP5 and CMIP6, respectively. To ensure consistent climate change impact assessments, observational and historical model outputs were aggregated to a common baseline period of 1995-2014, as utilized in the IPCC Sixth Assessment Report (AR6). The climate scenarios employed in the ISI-MIP consist of a combination of Representative Concentration Pathways (RCP) and Shared Socioeconomic Pathways (SSP). Their detailed information is listed in Table S1 in Supporting Information S1. For this study, 3 future SSP scenarios (SSP1-2.6, SSP3-7.0, and SSP5-8.5) were selected for the periods 2021-2040, 2041-2060, 2061-2080, and 2081-2100 (Ullah et al., 2022). These scenarios provide a broad range of potential future climates, covering weak, moderate, and strong forcing. The raw outputs from the 5 GCMs mentioned above were downscaled to a horizontal resolution of 0.5° × 0.5° using a statistical downscaling algorithm. This process involved bias revisions based on multiple reliable observations and reanalysis data, while preserving the long-term climate trends present in the GCM raw results. The processed results have been widely applied in the study of changes in extreme climate events and their impacts, serving as inputs to various assessment models within the ISI-MIP framework. In order to reduce prediction uncertainties, the field of climate change prediction commonly employs multi-model ensemble averaging. This study also focuses on the results of multi-model ensemble averaging (MME) to assess reliability. Given the lack of high-resolution and spatial-temporal continuity in instrumental records within the study area, The CRU dataset was adopted as observational data for the study area. It is important to note that while this dataset is referred to as observational data, it is not strictly derived from instrumental observational records.

The Land Use Harmonization Version 2 (LUH2) dataset is employed in this study to represent historical and future land use activities worldwide from the year 850 to 2100. The dataset has been widely utilized and referenced (Chen et al., 2020; Ma et al., 2020; Hurtt et al., 2020; Eyring et al., 2016) and serves as a significant land use forcing dataset for CMIP6 (Eyring et al., 2016). LUH2 was developed based on the Global Environmental History Database (HYDE) and incorporates multiple future scenarios aligned with the SSP framework (García-Peña et al., 2021). It provides globally gridded partial land use patterns, base land use transitions, key agricultural management information, and secondary land data spanning the period from 850 to 2100. The dataset has a spatial resolution of 0.25° × 0.25° and a temporal resolution of 1 year (García-Peña et al., 2021; Song et al., 2021). Within LUH2, land is classified into five main land use types (agricultural, rangeland, primary, secondary, and urban), each comprising twelve subtypes. For the representation of cropland, the sum of C3ann, C3per, C4ann, C4per, and C3nfx was utilized. In order to ensure consistency between datasets, the cropland data were interpolated to a resolution of 0.5° × 0.5° using a bilinear interpolation method, aligning it with the resolution of the climate data.

Future population data for the period 2020-2100 under different SSP scenarios were acquired from the NASA Socioeconomic Data and Applications Center (SEDAC) (Zhang et al., 2022).

It is important to note that the temporal resolution of the SEDAC population data is 10 years. Consequently, for this study, we used the average population values in 2020, 2030, 2040, 2050, 2060, 2070, 2080, 2090, and 2100 to represent the future population from 2020 to 2100. In order to maintain a consistent resolution between the population and climate datasets, the population data was interpolated to a resolution of 0.5° × 0.5° using a bilinear interpolation technique, ensuring alignment with the resolution of the climate data.

Table 1 Details of the ISI-MIP climate models used in this study.

Model name	Institution ID	Resolution	Country
GFDL-ESM4	Geophysical Fluid Dynamics Laboratory	1°×1.25°	USA
IPSL-CM6A-LR	Institut Pierre Simon Laplace	1.2676°×2.5°	France
MPI-ESM1-2-HR	Max Planck Institute for Meteorology	1.865°×1.875°	Germany
MRI-ESM2-0	Meteorological Research Institute	1.124°×1.125°	Japan
UKESM1-0-LL	National Centre for Atmospheric Science and Met Office Hadley Centre	1.25°×1.875°	UK

2.3 Evaluation methods for datasets

Taylor diagrams (Taylor, 2001) provide a comprehensive assessment of a model's ability to reproduce spatial patterns of climate variables, making them a widely used method for evaluating climate model performance and dataset suitability (Guo et al., 2021; Yue et al., 2021; Sun et al., 2021). In this study, we compared the data from five climate models and a multi-model ensemble mean with observed data (see Figure S1 in Supporting Information S1). The Taylor diagrams present correlation coefficients (R), central root mean square error (RMS), and standard deviation (SD) for each climate model, the multi-model ensemble average, and the observations in a single plot, illustrating the level of agreement between the model datasets and the observations. Furthermore, we assessed the model dataset's performance at a monthly scale by calculating precipitation for each month and comparing it to the observed data (see Figure S2 in Supporting Information S1). The closer the model data align with the observations, the higher their accuracy. By employing the Taylor diagram method, we comprehensively evaluated the accuracy of the CA climate model and its performance at the monthly scale. This approach enables the selection of the most suitable dataset, serving as the best alternative to observed data for characterizing future EPEs (see Figure S3 in Supporting Information S1).

2.4 Definition and Characteristics of Extreme Precipitation Events

The hazard metric employed in this study is the annual number of days with extreme precipitation, which serves as an indicator of the frequency of such events. Extreme precipitation is defined as daily rainfall exceeding a specific threshold. Previous studies commonly utilized extreme precipitation indices with fixed absolute thresholds specific to the study area (Raymond et al., 2020). However, the hazard associated with extreme events is influenced by various factors such as event characteristics, geographical conditions,

infrastructure, and population awareness. For instance, even small amounts of precipitation in arid and semi-arid regions can lead to floods and landslides, rendering absolute thresholds insufficient for capturing the true hazard of extreme precipitation in these regions. Consequently, we employed relative thresholds, specifically the 95th percentile (Thackeray et al., 2022; Alexander et al., 2019) of wet days (precipitation > 1 mm/day) for each grid cell. Relative thresholds consider regional differences in precipitation by accounting for regional and seasonal factors, thereby determining location-specific thresholds based on the actual precipitation conditions at each location. This approach is more suitable for capturing regional spatial and temporal variability and assessing exposure changes due to the significant climatic variations across the globe (Liu et al., 2017). In this study, we introduced four extreme precipitation indices to characterize EPEs and analyze their variability (Chen et al., 2013; Gimeno et al., 2022; Wang, 2005; Mondal et al., 2022):

1. Total Extreme Precipitation (TEP) is defined as the cumulative annual precipitation (in mm) exceeding the threshold value.

2. Extreme Precipitation Event Frequency (EPEF) corresponds to the number of days (in days) in a year associated with EPEs.

3. Extreme Precipitation Event Intensity (EPEI) is defined as the average daily precipitation (in mm/day) per grid cell during an extreme precipitation event.

4. Extreme Precipitation Event Impact Area (EPEA) corresponds to the maximum impacted area (in km²) by an extreme precipitation event.

2.5 Cropland and Population exposure to Extreme Precipitation Events

Population and cropland exposure in this study is quantified as the product of the number of days with extreme precipitation, the population exposed, and the cropland area within each grid cell (Zhang et al., 2022; Sun et al., 2023; Wang et al., 2023; Jones et al., 2015). The resulting units are person-days of exposure and square kilometers of cropland exposed. To account for interannual variability, exposure for future periods was determined by calculating a 20-year average of annual extreme precipitation days and utilizing population and cropland projections. The average annual exposure was then computed for each grid cell and aggregated to provide an overall assessment for CA.

$$E_{pop} = \frac{\sum_{m=1}^{20} C_m \times P}{20} \quad (1)$$

$$E_{crop} = \frac{\sum_{m=1}^{20} C_m \times G}{20} \quad (2)$$

where E_{pop} and E_{crop} are indicates the 20 years mean of population exposure (person-days) and cropland exposure (km^2), m denotes the mth year of the base period, C and P represents the total number of annual EPEF and simulated population number in person, while cropland simulation denoted by G.

2.6 Relative Changes in Exposure

To determine the relative contributions of climatic, population, and cropland to the total exposure. The variations in climatic, population, and cropland exposures were decomposed with respect to the climatic effect, population effect, cropland effect, and the interaction effect, respectively (Chen et al., 2020; Jones et al., 2015). Generally, the influence of population and cropland was estimated by holding climate constant while changing population. Similarly, the population and cropland were set as constant while computing the climate effect. The interaction effect was intended to describe the regions with a growing population and cropland approaches toward EPEF under changing climate. The changes in climate, population, and cropland exposure were decomposed using Equation 3 and Equation 4.

$$\Delta E_{pop} = C_r \times \Delta P + P_r \times \Delta C + \Delta P \times \Delta C \quad (3)$$

$$\Delta E_{crop} = C_r \times \Delta G + G_r \times \Delta C + \Delta G \times \Delta C \quad (4)$$

where ΔE_{pop} and ΔE_{crop} are the total changes in population and cropland exposures, C_r, P_r, and G_r indicates the total annual EPEF, population, and cropland for the reference period (2021-2040), respectively. Whereas ΔC, ΔP, and ΔG are the changes in annual EPEF, population, and cropland, respectively. Hence, the population effect is $C_r \times \Delta P$, the cropland effect is $C_r \times \Delta G$, the climate effects are represented by $P_r \times \Delta C$ and $G_r \times \Delta C$, and the interaction effects are the $\Delta P \times \Delta C$ and $\Delta G \times \Delta C$. To calculate the percentage change for each effect, we divide the above equation by the exposure in the reference period.

3. Results

3.1 Future Changes in Cropland and Population

The spatial distribution of the projected changes in CA cropland and the temporal characteristics of cropland area changes under three future scenarios (SSP1-2.6, SSP3-7.0, and SSP5-8.5), and four defined time periods are presented in Figure 2. Examining the spatial distribution (Figure 2a-l), cropland in CA displays a high degree of consistency across all scenarios, primarily concentrated in northern Kazakhstan, southern Tajikistan, and northern Kyrgyzstan. The line graph depicts the temporal changes in cropland area, indicating a decreasing trend in recent years for both the SSP1-2.6 and SSP3-7.0 scenarios. Conversely, the SSP5-8.5 scenario demonstrates a pattern of increasing and then decreasing cropland in CA. In terms of overall change in cropland area, the largest area is projected under the SSP5-8.5 scenario, followed by SSP1-2.6, with SSP3-7.0 exhibiting the smallest cultivated area. Assessing the rate of change reveals that the SSP3-7.0 scenario has the highest rate, followed by SSP1-2.6, while SSP5-8.5 exhibits the lowest rate. Between 2041-2060, noticeable changes in cropland area are observed in the border regions of northern and eastern Kazakhstan, Tajikistan, and Kyrgyzstan under the SSP1-2.6 (Figure 2b) and SSP3-7.0 scenarios (Figure 2f). In the SSP3-7.0 scenario, the most pronounced change in cultivated area within CA is evident, with a decrease from 330,000 km² in 2021-2040 (Figure 2e) to 290,000 km² in 2041-2060 (Figure 2f), primarily driven by the reduction of cultivated land in northern Kazakhstan.

Subsequently, the area increases to 310,000 km² in 2081-2100 (Figure 2h). Understanding and accounting for these divergences between projected SSPs is crucial to comprehensively investigate the impact of future climate risks, such as EPEs, on cropland.

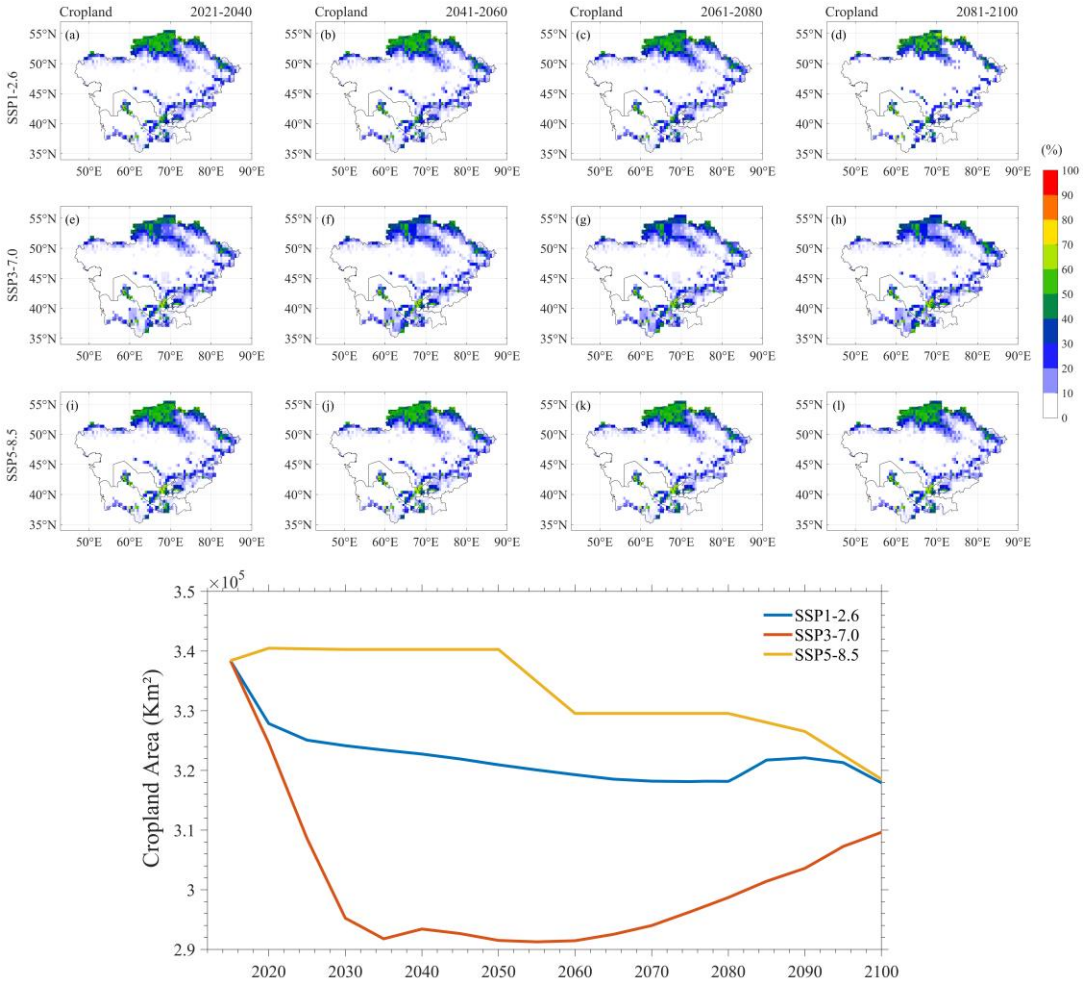

Figure 2. Spatial distributions of 20-year average cropland area share and projected cropland for four defined future periods under SSP1-2.6, SSP3-7.0 and SSP5-8.5 scenarios. Line plots depict the total cropland area of Central Asia (CA) for the period 2020-2100.

The spatial and temporal changes in the population of CA under future scenarios and four selected time periods are shown in Figure 3. CA exhibits a highly heterogeneous spatial distribution of population density, making it one of the regions with notable variation globally. The spatial map (Figure 3a-l) reveals that the distribution of population in CA aligns closely with the distribution of cropland across all scenarios, concentrating primarily in northern Kazakhstan, southeastern Uzbekistan, northwestern Tajikistan, and western Kyrgyzstan. The line graph illustrates that under the SSP3 scenario, the population is projected to consistently increase in each future time period. In contrast, the populations under the SSP1 and SSP5 scenarios display a pattern of growth followed by a decline. These findings indicate that the population size of CA exhibits greater variability under future scenarios. Regarding population size, SSP3 exhibits the largest population, followed by SSP1, while SSP5 has the smallest population. Spatially, the distribution of population in CA is highly uneven. Although Kazakhstan boasts the largest land area, its population size falls significantly behind that of

Tajikistan and Uzbekistan. In fact, the population in CA is predominantly concentrated in Tajikistan and Uzbekistan. Under the SSP1 and SSP5 scenarios, the population size peaks in 2040 at 70 and 65 million people, respectively, before gradually decreasing in subsequent years. In the SSP3 scenario, the population of CA reaches its maximum, steadily increasing over time to approximately 100 million people by 2100.

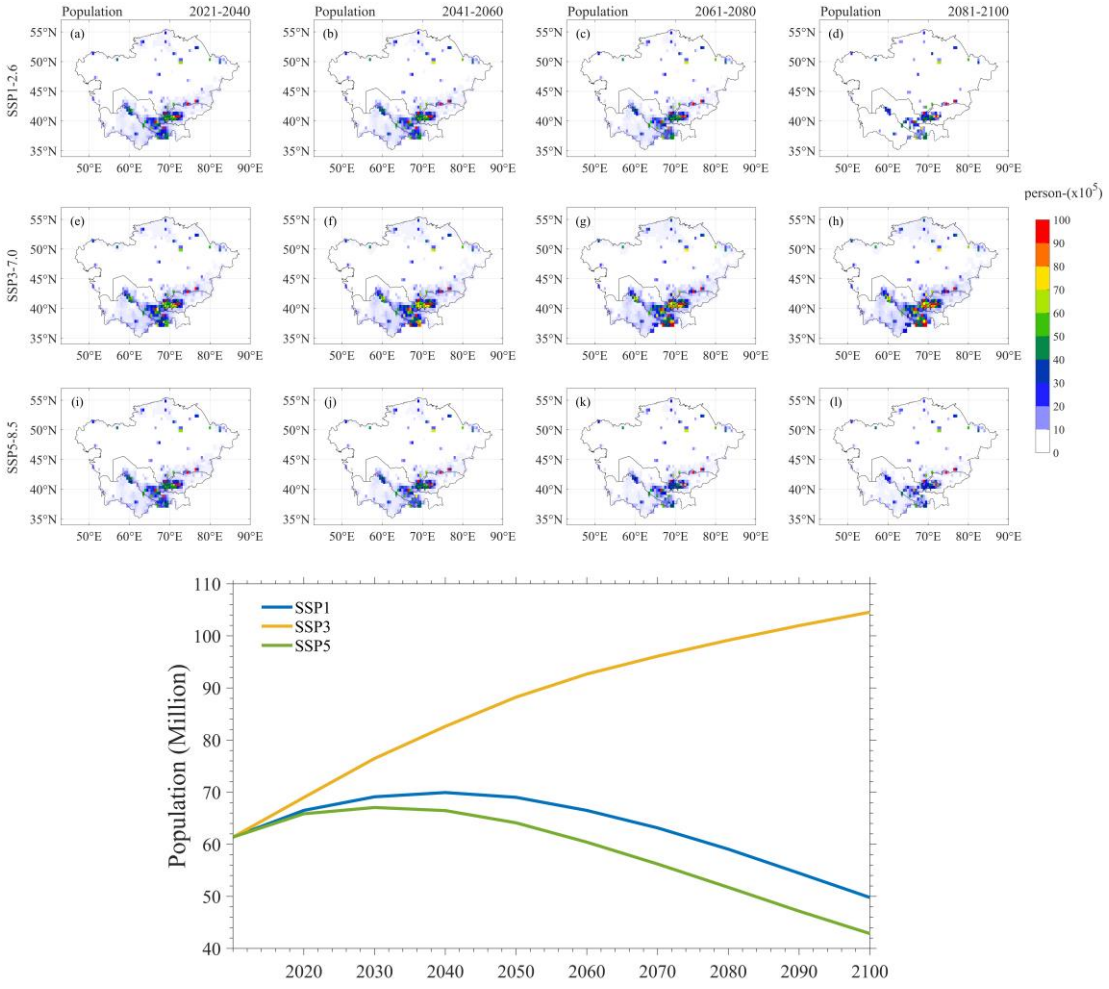

Figure 3. Spatial distributions of 20-year average number of population and projected population for four defined future periods under SSP1-2.6, SSP3-7.0 and SSP5-8.5 scenarios. Line plots depict the total population of Central Asia (CA) for the period 2020-2100.

3.2 Characteristics of extreme precipitation events under different future scenarios

The projected changes in the characteristics of EPEs in CA for the period 2020-2100 are presented in Figure 4. The findings highlight that higher emission scenarios will intensify EPEs, leading to potentially catastrophic consequences for the economy and society. The analysis reveals varying increases in EPEs under the SSP1-2.6, SSP3-7.0, and SSP5-8.5 scenarios (Figure 4a). Overall, SSP5-8.5 exhibits the highest magnitude of extreme precipitation, approaching a maximum value of 60 mm, followed by SSP3-7.0, with the smallest impact observed under SSP1-2.6. Moreover, the severity of EPEs amplifies over time. Examining the frequency characteristics of EPEs (Figure 4b), a similar pattern emerges as observed in extreme precipitation. Under the medium and high emission scenarios (SSP3-7.0 and SSP5-8.5), EPEs occur more frequently compared to the SSP1-2.6 scenario. Notably, the increase in event

frequency is more pronounced in SSP3-7.0 and SSP5-8.5, exhibiting a clear upward trend over time. The SSP5-8.5 scenario presents an especially drastic rise in extreme precipitation frequency (Figures 4b and 4c). Regarding the intensity of EPEs (Figure. 4c), distinct variations are observed across different scenarios. The SSP5-8.5 scenario exhibits significantly higher intensity compared to SSP3-7.0 and SSP1-2.6. These findings emphasize that what was once considered rare in the past may become the norm in the future under high emission scenarios. In summary, increasing emission scenarios will result in more frequent and prolonged EPEs in CA in the coming decades. These findings underscore the urgent need for proactive measures to mitigate the potential impacts of these events on the region.

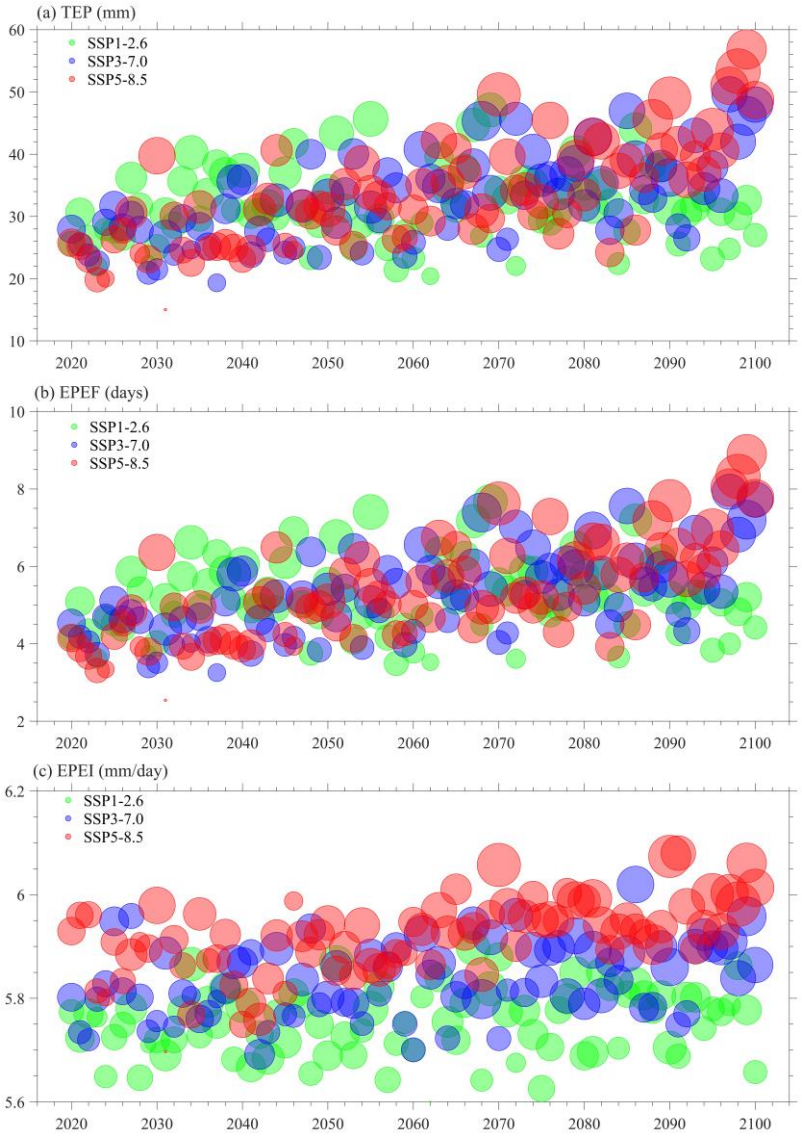

Figure 4. Projected temporal changes in extreme precipitation events characteristics from 2020 to 2100 under the SPP1-2.6, SSP3-7.0, and SSP5-8.5 scenarios over Central Asia (CA). (a) TEP, (b) EPEF, (c) EPEI. Bubble size indicates the EPEA.

Figure 5 presents the spatial distribution of predicted regional average changes in extreme precipitation event characteristics (extreme precipitation amount, frequency, and intensity) for the entire South Asia region during the period 2020-2100, under three future scenarios: SSP1-

2.6, SSP3-7.0, and SSP5-8.5. The box plots in the Figures illustrate the variations across these scenarios. The spatial distribution of extreme precipitation amounts (Figures 5a, 5d, and 5g), frequencies (Figures 5b, 5e, and 5h), and intensities (Figures 5c, 5f, and 5i) exhibits a similar pattern for all three scenarios. EPEs are widespread throughout the CA region, excluding central Kazakhstan and northern Uzbekistan. The primary areas experiencing EPEs in CA are the southern Tien Shan Mountains and northern Kazakhstan. Under different future climate scenarios, the range of EPEs in CA expands, with higher values of extreme precipitation and intensity occurring in the border regions of Tajikistan, Kyrgyzstan, and Uzbekistan. Additionally, elevated values of extreme precipitation frequency are observed in the northern part of Kazakhstan, alongside the southeastern region of CA. In summary, EPEs in CA concentrate in densely populated areas and regions with significant cropland distribution. This exacerbates the impact of extreme precipitation on both the population and cropland in CA.

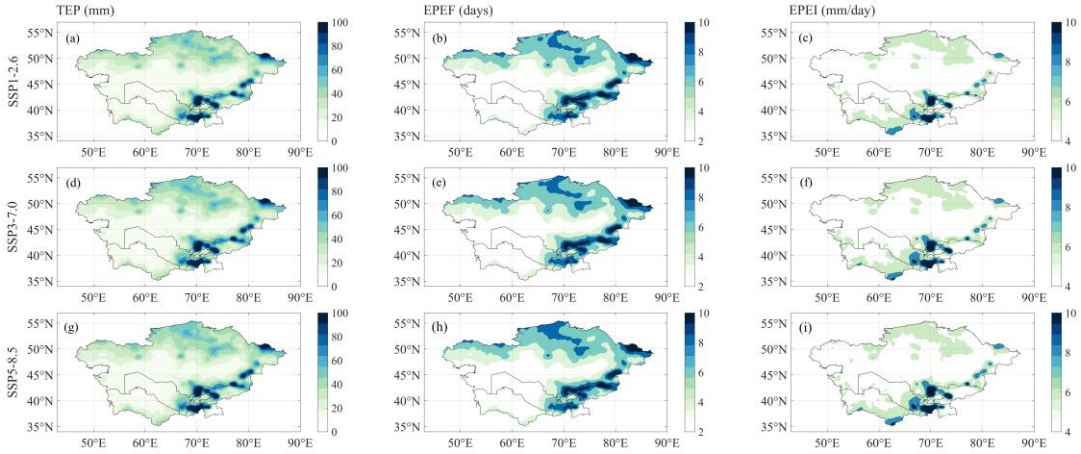

Figure 5. Projected spatial changes in extreme precipitation events characteristics under the SPP1-2.6, SSP3-7.0, and SSP5-8.5 scenarios over Central Asia (CA). (a, d, and g) TEP, (b, e, and h) EPEF, (c, f, and, i) EPEI.

Figure 6 illustrates the spatial distribution of future trends in the characteristics of EPEs in CA, projected for the period 2020-2100, under three future scenarios: SSP1-2.6, SSP3-7.0, and SSP5-8.5. In the SSP1-2.6 scenario (Figures. 6a-c), most of CA exhibits a drying trend, with notable wetting areas concentrated in the northern part of CA, northern Kazakhstan, and the southern Tien Shan Mountains. Conversely, the SSP3-7.0 scenario (Figures. 6d-f) reveals an expansion of wetting areas across a large portion of CA, resulting in significant wetting effects. Under the SSP5-8.5 scenario (Figure. 6g-i), extreme precipitation, as well as the frequency and intensity of EPEs, demonstrate a substantial increase over the majority of CA, particularly in mountainous regions. The findings indicate that the overall increase in EPEs in CA exceeds 90% in the medium and long term under the SSP3-7.0 and SSP5-8.5 scenarios. In general, it can be inferred that the projected future changes in extreme precipitation in CA, specifically under the SSP5-8.5 scenario, are significant, ranging from 80% to 90%, with the highest magnitudes observed in mountainous regions and the lowest in plains.

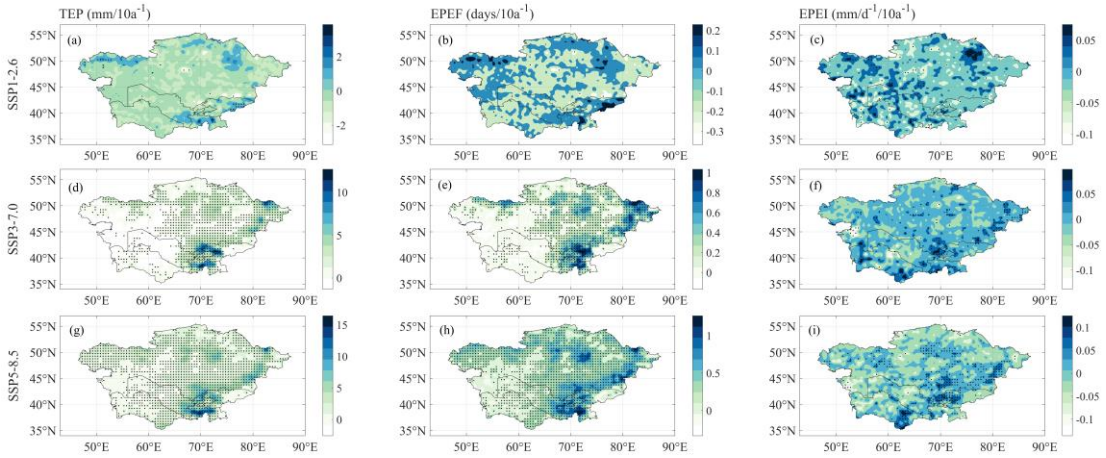

Figure 6. Projected spatial changes of trends in extreme precipitation events characteristics under the SPP1-2.6, SSP3-7.0, and SSP5-8.5 scenarios over Central Asia (CA). (a, d, and g) TEP, (b, e, and h) EPEF, (c, f, and, i) EPEI.

3.3 Cropland and Population Exposures to Extreme Precipitation Events

The spatial distribution of cropland exposure to EPEs under the three SSP scenarios (SSP1-2.6, SSP3-7.0, and SSP5-8.5) and the four defined time periods across CA are presented in Figure 7. Additionally, it illustrates the temporal variation in total cropland exposure to EPEs. In the SSP1-2.6 scenario, regions such as northern Kazakhstan, northern Kyrgyzstan, and northern Tajikistan exhibit faster increases in medium- and long-term cropland exposure to EPEs, affecting an area of over 250,000 km² (Figures 7a-d). However, under the same scenario, a more prolonged and detrimental surge in cropland exposed to extreme precipitation risk is expected in northern and eastern Kazakhstan in the long term. Under the SSP3-7.0 scenario (Figures 7e-h), cropland exposure increases more rapidly in the northeastern regions of Kazakhstan and the border areas of Tajikistan and Kyrgyzstan. In the case of SSP5-8.5, higher cropland exposure is observed during the long-term period compared to the other time periods (Figures 7i-l). Analyzing the 2021-2040 time period, cropland exposure under the low emission scenario is approximately 45.6 million km², significantly higher than the 34.8 million km² and 38.8 million km² under the medium and high emission scenarios, respectively. Total cropland exposure increases significantly over time, with the exposure in the SSP5-8.5 scenario reaching 56.8 million km² by 2081-2100, notably higher than the exposure in the SSP3-7.0 scenario (48.4 million km²) and the SSP1-2.6 scenario (44.6 million km²). Interestingly, large-scale population exposure is not projected in central Kazakhstan, northern Uzbekistan, northern Turkmenistan, Tajikistan, and southeastern Kyrgyzstan. This can be attributed to the absence of future EPEs in these regions and the fact that most of these areas are characterized by desert and alpine mountain landscapes with limited cropland distribution. Regional sums indicate that cropland exposure to EPEs increases by 25.7%, from 119.2 million km² in 2021-2040 to 149.8 million km² in 2081-2100, with the highest exposure observed in the SSP5-8.5 scenario at approximately 190.7 million km², followed by SSP1-2.6 (182.1 million km²) and SSP3-7.0 (164.2 million km²). Regarding the time period, the highest cropland exposure to EPEs is projected for 2081-2100. Differences in population exposure to EPEs under the same scenarios may be attributed to variations in the frequency of such events. These findings align with the

spatial distribution of cropland exposed to EPEs in the selected scenarios.

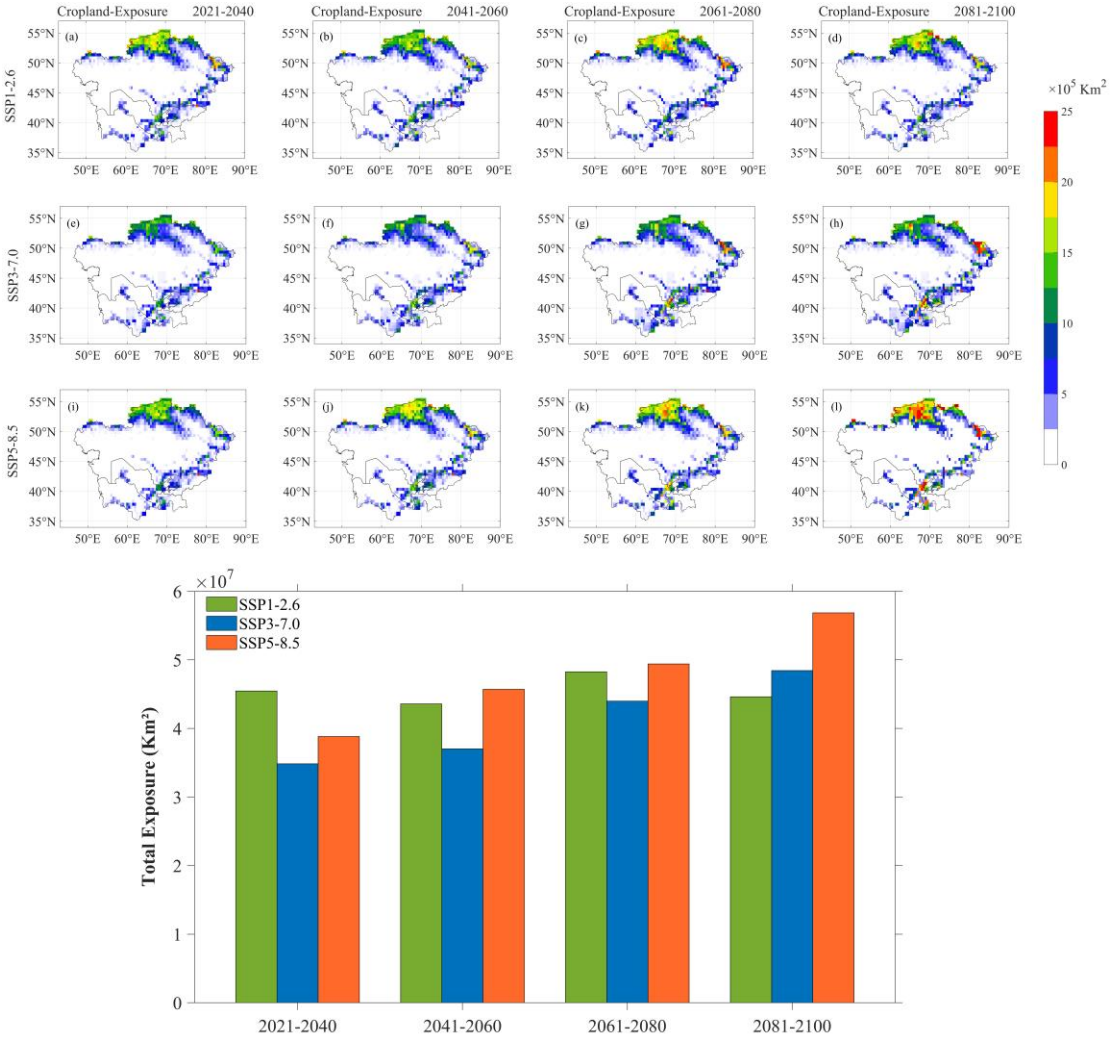

Figure 7. Projected changes in cropland exposure to extreme precipitation events under the SSP1-2.6, SSP3-7.0 and SSP5-8.5 scenarios and four-time periods across Central Asia (CA). Bar plots depict the total area affected by extreme precipitation events for four different time periods and across CA.

The spatial pattern of projected changes in population exposure to EPEs in CA across four time periods under three future scenarios are shown in Figure 8. In all three scenarios, population exposure shows a slight increase in the short term (Figure 8a, Figure 8e, and Figure 8i). However, over time, population exposure gradually rises under the high emission scenario. The areas with high population exposure in CA are concentrated in northwestern Tajikistan, western Kyrgyzstan, and southeastern Uzbekistan, with a smaller distribution in the northern part of Kazakhstan. Bar charts represent the total population exposure in CA for all three scenarios and four time periods. In the SSP1-2.6 scenario, population exposure exhibits a decreasing trend over time. Under the SSP3-7.0 scenario, population exposure to EPEs exceeds 48.1 billion person-days, with the most significant change occurring in northwestern Tajikistan, western Kyrgyzstan, and southeastern Uzbekistan. In these regions, exposure increases by 92.6%, resulting in a total population exposure of around 8.1 billion person-days in 2021-2040, escalating to approximately 15.6 billion person-days in 2081-2100. Population exposure under

the SSP5-8.5 scenario and the SSP1-2.6 scenario is roughly comparable, with population exposure under the SSP1-2.6 scenario being higher than that under the SSP5-8.5 scenario until the 2061-2080 time period. In conclusion, the main factor contributing to the increase in population exposure to EPEs in CA is future population growth. It is noteworthy that large-scale population exposure is not observed in central Kazakhstan, northern Uzbekistan, northern Turkmenistan, Tajikistan, and southeastern Kyrgyzstan, likely due to the presence of uninhabited areas in these regions. The highly heterogeneous population distribution in CA, with population densities reaching up to 70 persons/km², exacerbates population exposure to EPEs to some extent.

Regional aggregations consistently demonstrate an increase in population exposure to EPEs across all scenarios, with the highest exposure observed under the SSP3-7.0 scenario at approximately 48.1 billion person-days, followed by SSP1-2.6 and SSP5-8.5. Regarding the time periods, total population exposure increases by 29.6% from 2021-2040 to 2081-2100. Population exposure to EPEs is highest in 2081-2100, followed by 2061-2080 and 2041-2060, with the lowest exposure occurring in 2021-2040. The disparities in population exposure under the same scenarios can be attributed to variations in the frequency of EPEs. These findings align with the spatial distribution of populations exposed to EPEs in the selected scenarios. In summary, population exposure to extreme precipitation is anticipated to undergo a substantial increase in response to future global warming. Even with early mitigation efforts, exposure levels are projected to rise across a significant portion of CA. This increase in exposure is largely attributable to the uneven distribution of populations in the region and poses significant threats to societies, ecosystems, and human well-being in the future. To effectively mitigate these threats, a thorough understanding of exposure changes is crucial for driving mitigation actions and addressing their underlying causes.

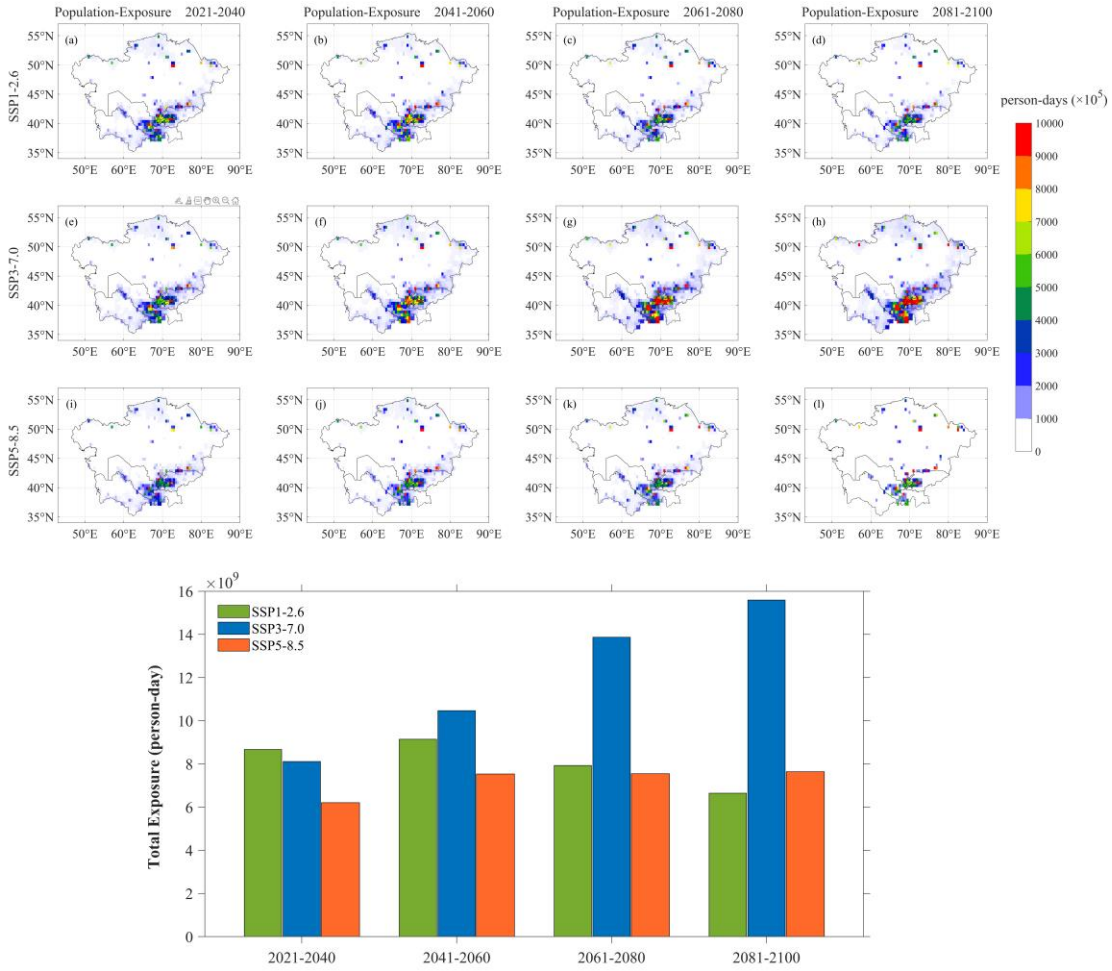

Figure 8. Projected changes in population exposure to extreme precipitation events under the SSP1-2.6, SSP3-7.0, and SSP5-8.5 scenarios and four-time periods across Central Asia (CA). Bar plots represent the total number of people affected by extreme precipitation events for four different time periods and across CA.

3.4 Exploring the Importance of Relative Changes in Exposure

To investigate the relative importance of different factors, we conducted a detailed analysis to determine the contribution of population and cropland exposure to the interaction components of CA. This analysis focused on climatic effects, population, cropland, and their interaction effects under three emission scenarios in the mid- to late 21st century. Examining the influences on cropland exposure (Figure 9), we observed consistent variation in the relative importance of climate change, cropland change, and their interaction effects across scenarios. These findings suggest that the increase in cropland exposure in CA is primarily controlled by the climate component. Under the SSP1-2.6 scenario, the relative changes in the cropland, climate, and interaction components of CA cropland exposure were 15.78%, 82.6%, and 1.61%, respectively. In this scenario, negative impacts from the population and interaction components are evident, with the increase in population exposure solely driven by the climate component. This is primarily due to the projected shrinkage of the cultivated area by the end of the 21st century, which, combined with the substantial impacts of climate change, counteracts the negative

increase. Notably, the climate component consistently outweighs the cropland component, but the change in the cropland component and the cropland-climate interaction component is increasing while the climate component is weakening. This is demonstrated by the fact that relative to the base period, from 2081-2100, the cropland and climate interaction components increase from 2.43% to 13.42%, and the cropland component increases from 15.78% to 26.35%, whereas the climate component decreases from 82.6% to 70.73% (see Table S2 in the Supporting Information). Interestingly, across all scenarios, the climate component tends to decrease over time, while the population and interaction effects tend to increase. Nevertheless, the climate effect consistently dominates in all scenarios, despite its decreasing trend.

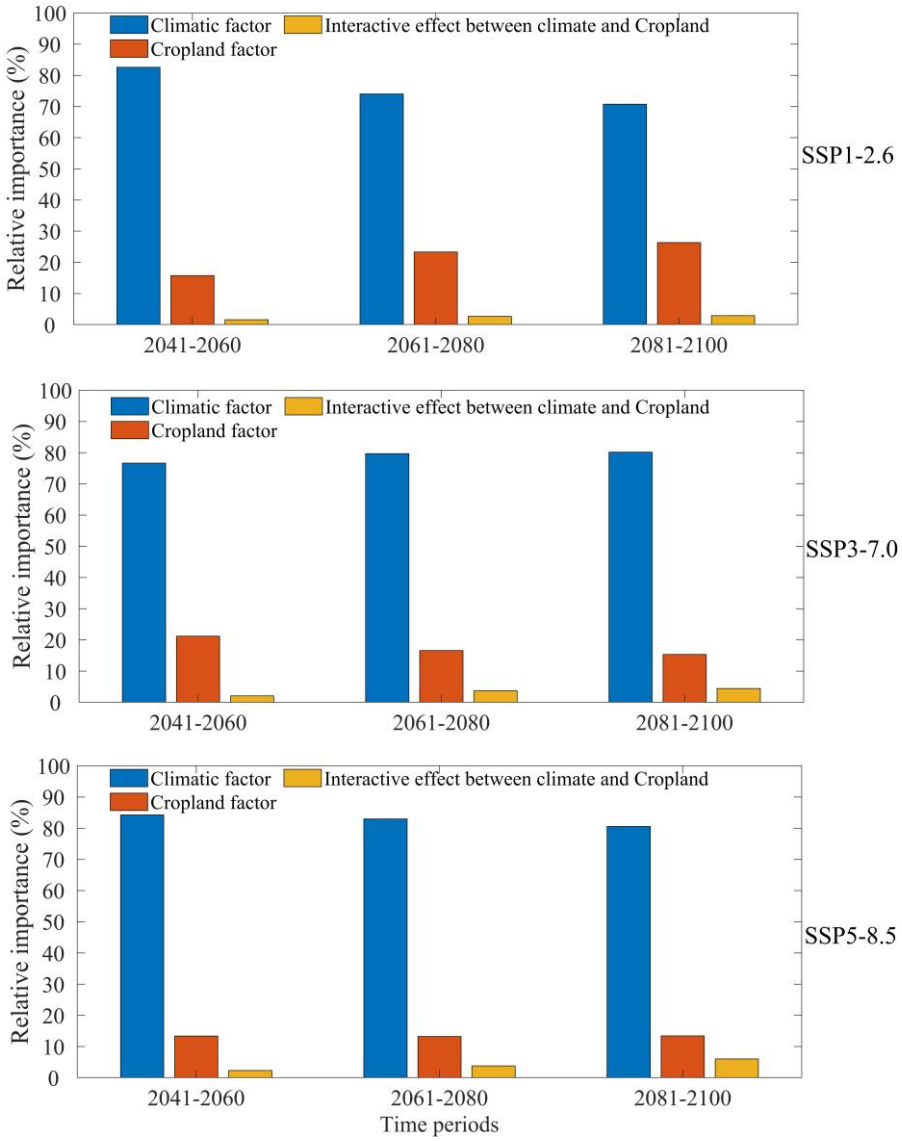

Figure 9. Different factors of the effects driving projected changes in cropland exposure to EPEF over Central Asia (CA) under SSP1-2.6, SSP3-7.0, and SSP5-8.5 scenarios and three-time periods.

Changes in population exposure to EPEs are influenced not only by variations in climatic factors but also by alterations in population size and its spatial distribution. Figure 10 depict the overall changes in population exposure and its contributing factors across CA for different

climate scenarios and three distinct time periods. The relative importance of climate change, population change, and their interaction effects exhibits significant variation throughout CA. Under the SSP1-2.6 scenario, changes in population exposure are primarily driven by demographic factors. In contrast, under both the SSP3-7.0 and SSP5-8.5 scenarios, climatic factors play a dominant role in determining population exposure. However, it is worth noting that the decline in climatic factors is more rapid under the SSP5-8.5 scenario compared to the SSP3-7.0 scenario. Importantly, population and climate interaction effects demonstrate a substantial increase across all scenarios, with their significance intensifying as emissions rise. For instance, the population and climate interaction effects experience an increase of 2.76%, 6.43%, and 11.62% for the SSP1-2.6, SSP3-7.0, and SSP5-8.5 scenarios, respectively (see Table S3 in the Supporting Information).

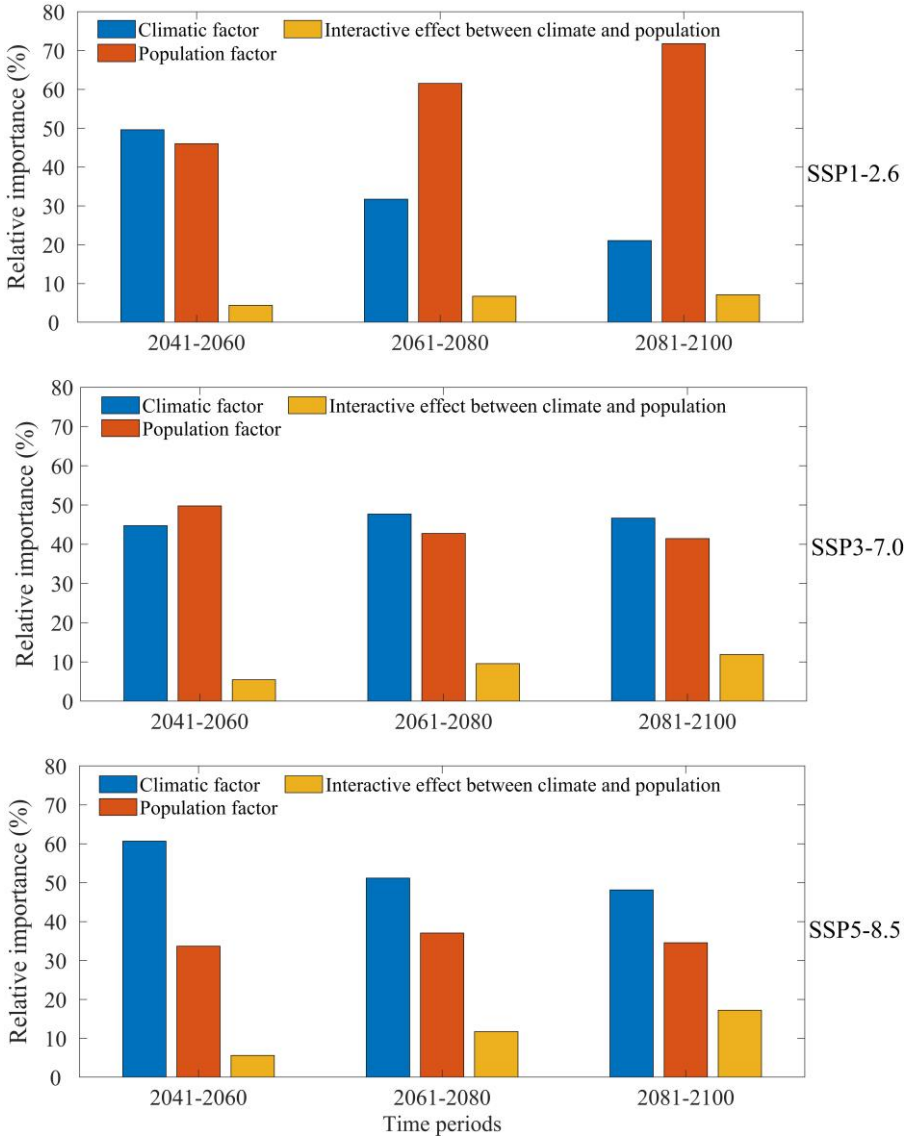

Figure 10. Different factors of the effects driving projected changes in population exposure to EPEF over Central Asia (CA) under SSP1-2.6, SSP3-7.0, and SSP5-8.5 scenarios and three-time periods.

4. Conclusions and Discussions

The primary objective of this study is to examine the projected changes in EPEs in CA and their implications for population and cropland exposure. To achieve this objective, the study utilizes the state-of-the-art ISI-MIP multi-model ensemble mean, incorporating three Shared Socioeconomic Pathway (SSP) scenarios (SSP1-2.6, SSP3-7.0, and SSP5-8.5) and four predetermined time periods (2021-2040, 2041-2060, 2061-2080, and 2081-2100). The analysis employs daily precipitation data from the multi-model ensemble mean to assess the future variability characteristics of EPEs in CA. Furthermore, population and cropland datasets corresponding to different SSP scenarios are utilized to investigate the changes in population and cropland exposure resulting from EPEs in the region. This study aims to achieve several key objectives. Firstly, it seeks to investigate the evolving characteristics of EPEs in CA throughout the 21st century. Secondly, it aims to assess the impacts of these events on the population and cropland in the region. Lastly, the influence of different factors (i.e., population, cropland, climate, and interaction) on EPEF and changes in socioeconomic exposure was further investigated. The study aims to provide regional evidence that can support policymakers in the development of appropriate climate change adaptation and mitigation strategies for EPEs.

Our study reveals three key findings. Firstly, the analysis demonstrates a broad consensus among climate models for various future scenarios, indicating a significant increase in population and cropland exposure to EPEs in CA throughout the 21st century. Contrary to the expectation of limited exposure due to scarce precipitation in the region, our findings suggest that the actual exposure is substantial. Consequently, policymakers and the research community need to acknowledge population and cropland changes as critical factors when assessing the risks associated with EPEs. Secondly, we identified that the highest exposure to extreme precipitation among the population in CA occurs under the SSP3-7.0 scenario, while the highest exposure for cropland is observed under the SSP5-8.5 scenario. Notably, both exposures exhibit a strong spatial similarity, primarily concentrating in the northern part of Kazakhstan and the southwestern part of CA. Lastly, our study highlights that EPEs in CA tend to concentrate on the windward slopes of the region's mountain ranges. These areas coincide with high population density and extensive distribution of cropland. The spatial exposure of population and cropland to extreme precipitation in CA displays a high degree of heterogeneity, warranting greater attention. Based on our findings, it is crucial to prioritize the reduction of greenhouse gas emissions to mitigate population and cropland exposure to extreme precipitation. Additionally, urgent action is required to design and implement effective adaptation measures that enhance preparedness and response to EPEs.

Moreover, we extensively investigate the changes in socioeconomic exposure to EPEF and their diverse effects on both local and regional scales within CA. This investigation is based on defined time periods and three distinct SSP scenarios. Overall, across all three future scenarios, the augmentation of cropland exposure in CA can be attributed to climate effects; however, it is noteworthy that the influence of climate effects is diminishing, while the impact of cropland forcing and cropland-climate interactions is increasing. As for population exposure, the predominant cause of future increases within CA is climate effects; nevertheless, the interaction between population and climate exhibits a substantial rise with escalating emissions and the

passage of time. Consequently, while the risk of extreme precipitation in CA is still primarily determined by future increases in precipitation, the significance of population and cropland factors should not be overlooked.

The future spatial and temporal patterns of EPEs in CA suggest that significant occurrences of such events are expected over most of CA under the SSP3-7.0 and SSP5-8.5 scenarios, with a notable expansion of extreme precipitation across the high mountainous regions. Recent studies on extreme climate projections in CA have been relatively scarce compared to other global regions and have primarily focused on the Paris Agreement targets (Zhang et al., 2022) and higher global warming scenarios (Zhang et al., 2020; Zhang et al., 2019). However, these studies have revealed that CA is transitioning from a warm and dry condition to a warm and relatively humid condition due to climate change and the intensification of the water cycle. Supporting these findings, our study anticipates an increase in EPEs in the high mountain regions of CA (Yao et al., 2021; Zou et al., 2021; Zhang et al., 2019; Liu et al., 2022). Despite the significance of extreme precipitation, there are few studies assessing the changes in population and cropland exposure to climate extremes in CA. Limited information is available on the spatial and temporal variability of population and cropland exposure to extreme precipitation in CA under different future scenarios and time periods. Our study aims to bridge these research gaps by quantifying the exposure of CA populations and croplands to extreme precipitation under the SSP1-2.6, SSP3-7.0, and SSP5-8.5 scenarios in the 21st century. Given that CA is predominantly agricultural with high population density and a strong dependence on the spatial distribution of water resources, the risks associated with extreme precipitation to the population and cropland in the region are heightened. The results of this study will stimulate further research into the internal mechanisms governing the interactions between climate change, land cover, and social activities. Moreover, our findings provide a scientific basis for mitigating the risks associated with extreme precipitation and ensuring sustainable economic and social development.

Although this study estimated future population and cropland exposure to EPEs in CA, it has certain limitations that require attention in future research. One limitation is the lack of consideration for socioeconomic and demographic characteristics of the population, such as income, education level, and age, which could influence the extent of exposure to extreme precipitation in CA (Chambers, 2020; Watts et al., 2021; Park et al., 2022). We suggest that future studies estimating population exposure should incorporate a more precise classification of the age structure of the population. Currently, various studies have focused on exposure to climate extremes; however, there is no standardized definition of exposure. Some studies employ a method that multiplies the occurrence of extreme events by the population size to estimate population exposure to climate extremes (Batibeniz et al., 2020). Others define exposure as the area where extreme climate surpasses a hazard threshold during a specific time period (Zhang et al., 2018; Sun et al., 2017), while some adopt an intensity-area-duration approach to reflect changes in exposure to hazard events (Wen et al., 2019; Su et al., 2018; Wang et al., 2019). These different definitions result in variations in estimates of population exposure and the socioeconomic impacts of extreme weather events. Consequently, it is crucial to establish a scientifically grounded and uniform definition of population exposure to extreme events, considering factors such as hazard, exposure, and vulnerability, to accurately assess the

risk of disasters. In a warmer future, moderate increases in precipitation can have positive effects on livelihoods and economic development, leading to an anticipated rise in irrigation water demand in CA under future climate and socioeconomic scenarios (Tian et al., 2020). Therefore, future research should focus on climate sensitivity analysis for CA, aiming to quantify the net impacts of changes in water availability and use, particularly under critical levels of global warming. Such assessments are critical for effective climate change mitigation and adaptation strategies in the region.

More frequent and intense EPEs pose a significant threat to both the global population and the global food supply (Thomas et al., 2015). This risk is particularly pronounced in arid and semi-arid regions, where water resources play a crucial role as both a determining factor and a limiting factor for development (Gessner et al., 2013; Li et al., 2019). It is imperative to plan and implement adaptation and mitigation measures to address the adverse effects of climate extremes in CA. These measures should encompass various strategies at the individual, community, and national levels. Ensuring widespread education about extreme precipitation and its associated hazards, along with providing essential resources such as food, clothing, and medical insurance, can help mitigate the risks involved. Furthermore, the implementation of afforestation initiatives and sustainable water use policies may effectively mitigate the risks associated with extreme precipitation in the region. At the governmental level, there is a need for multilateral climate agreements and enhanced communication and cooperation among the five CA countries to collectively address the challenges posed by extreme climate hazards (Chen et al., 2021). Additionally, the increasing occurrence of extreme precipitation in arid and semi-arid zones may potentially alleviate water stress in these regions if properly harnessed. It is widely recognized that accelerated climate change can have catastrophic consequences, and exploring the utilization of extreme precipitation in arid zones from a new perspective represents an important avenue for future research.

Conflict of Interest

The authors declare no conflicts of interest relevant to this study.

Data Availability Statement

All data used in this study are available online. The CRU precipitation products are available from https://crudata.uea.ac.uk/cru/data/hrg/cru_ts_4.07/cruts.2304141047.v4.07/pre/. The Cropland data from 2020 to 2100 under different SSP scenarios is available from https://luh.umd.edu/data.shtml. The population data from 2020 to 2100 under different SSP scenarios can be obtained from the website of https://sedac.ciesin.columbia.edu/data/set/popdynamics-1-km-downscaled-pop-base-year-projection-ssp-2000-2100-rev01. The ISI-MIP model simulations are available from https://data.isimip.org/10.48364/ISIMIP.842396.1.

Acknowledgments

This research was jointly supported by the Key R&D Program of Xinjiang Uygur Autonomous Region (Grant No. 2022B03021), the Tianshan Talent Training Program of Xinjiang Uygur Autonomous region (Grant No. 2022TSYCLJ0011), Transformation of Scientific and

Technological Achievements from the Qinghai Province (Grant No. 2020-SF-145), the 2020 Qinghai Kunlun talents -Leading scientists project (Grant No. 2020-LCJ-02), and Key program of International Cooperation, Bureau of International Cooperation, Chinese Academy of Sciences (Grant No. 131551KYSB20210030). We are thankful to the CRU, ISI-MIP, SEDAC, and LUH2 groups for providing research data.

Author contributions

Conceptualization: Anming Bao, Tao Li **Formal analysis:** Tao Li, Jiayu bao **Funding acquisition:** Anming Bao **Methodology:** Tao Li, Fengjiao Song, Jinyu Chen **Software:** Tao Li, Jiayu bao, Ye Yuan **Supervision:** Anming Bao, Ye Yuan **Visualization:** Tao Li, Jiayu bao **Writing - original draft:** Tao Li, Jiayu bao, Fengjiao Song, Ye Yuan **Writing – review & editing:** Anming Bao, Xiaoran Huang, Tao Yu, Gang Long, Jingyu Jin, Diwen Dong, Naibi Sulei, Ting Wang

References

Alexander, L.V., Fowler, H.J., Bador, M., Behrangi, A., Donat, M.G., Dunn, R., et al. (2019). On the use of indices to study extreme precipitation on sub-daily and daily timescales. *Environmental Research Letters*, 14(12): 125008, https://doi.org/10.1088/1748-9326/ab51b6.

Basile, S.M.L., Tognetti, J.A., Gandini, M.L., Rogers, W.J. (2022). Climate change in the temperature and precipitation at two contrasting sites of the argentinean wheat region. *Theoretical and Applied Climatology*, 148(1-2): 237-254, https://doi.org/10.1007/s00704-022-03936-6.

Batibeniz, F., Ashfaq, M., Diffenbaugh, N.S., Key, K., Evans, K.J., Turuncoglu, U.U., et al. (2020). Doubling of u.s. Population exposure to climate extremes by 2050. *Earth's Future*, 8(4), https://doi.org/10.1029/2019EF001421.

Chambers, J. (2020). Global and cross-country analysis of exposure of vulnerable populations to heatwaves from 1980 to 2018. *Climatic Change*, 163(1): 539-558, https://doi.org/10.1007/s10584-020-02884-2.

Chen, H., Sun, J. (2021). Significant increase of the global population exposure to increased precipitation extremes in the future. *Earth's Future*, 9(9), https://doi.org/10.1029/2020EF001941.

Chen, J., Liu, Y., Pan, T., Ciais, P., Ma, T., Liu, Y., et al. (2020). Global socioeconomic exposure of heat extremes under climate change. *Journal of Cleaner Production*, 277: 123275, https://doi.org/10.1016/j.jclepro.2020.123275.

Chen, M., Vernon, C.R., Graham, N.T., Hejazi, M., Huang, M., Cheng, Y., et al. (2020). Global land use for 2015–2100 at 0.05° resolution under diverse socioeconomic and climate scenarios. *Scientific Data*, 7(1), https://doi.org/10.1038/s41597-020-00669-x.

Chen, Y., Zhai, P. (2013). Persistent extreme precipitation events in china during 1951-2010. *Climate Research*, 57(2): 143-155, https://doi.org/10.3354/cr01171.

Cho, C., Li, R., Wang, S.Y., Yoon, J., Gillies, R.R. (2016). Anthropogenic footprint of climate change in the june 2013 northern india flood. *Climate Dynamics*, 46(3-4): 797-805, https://doi.org/10.1007/s00382-015-2613-2.

Cook, B.I., Mankin, J.S., Marvel, K., Williams, A.P., Smerdon, J.E., Anchukaitis, K.J. (2020). Twenty‐first century drought projections in the cmip6 forcing scenarios. *Earth's Future*, 8(6), https://doi.org/10.1029/2019EF001461.

Devkota, K.P., Manschadi, A.M., Devkota, M., Lamers, J.P.A., Ruzibaev, E., Egamberdiev, O., et al. (2013). Simulating the impact of climate change on rice phenology and grain yield in irrigated drylands of central asia. *Journal of Applied Meteorology and Climatology*, 52(9): 2033-2050, https://doi.org/10.1175/JAMC-D-12-0182.1.

Dike, V.N., Lin, Z., Fei, K., Langendijk, G.S., Nath, D. (2022). Evaluation and multimodel projection of seasonal precipitation extremes over central asia based on cmip6 simulations. *International Journal of Climatology*, 42(14): 7228-7251, https://doi.org/10.1002/joc.7641.

Doan, Q.V., Chen, F., Kusaka, H., Dipankar, A., Khan, A., Hamdi, R., et al. (2022). Increased risk of extreme precipitation over an urban agglomeration with future global warming. *Earth's Future*, 10(6), https://doi.org/10.1029/2021EF002563.

Donat, M.G., Lowry, A.L., Alexander, L.V., O Gorman, P.A., Maher, N. (2016). More extreme precipitation in the world's dry and wet regions. *Nature Climate Change*, 6(5): 508-513, https://doi.org/10.1038/nclimate2941.

Eyring, V., Bony, S., Meehl, G.A., Senior, C.A., Stevens, B., Stouffer, R.J., et al. (2016). Overview of the coupled model intercomparison project phase 6 (cmip6) experimental design and organization. *Geoscientific Model Development*, 9(5): 1937-1958, https://doi.org/10.5194/gmd-9-1937-2016.

Fu, J., Jian, Y., Wang, X., Li, L., Ciais, P., Zscheischler, J., et al. (2023). Extreme rainfall reduces one-twelfth of china's rice yield over the last two decades. *Nature Food*, 4(5): 416-426, https://doi.org/10.1038/s43016-023-00753-6.

Gao, C., Su, B., Krysanova, V., Zha, Q., Chen, C., Luo, G., et al. (2020). A 439-year simulated daily discharge dataset (1861-2299) for the upper yangtze river, china. *Earth System Science Data*, 12: 378-402, https://doi.org/https://doi.org/10.5194/essd-12-387-2020.

García-Peña, G.E., Rubio, A.V., Mendoza, H., Fernández, M., Milholland, M.T., Aguirre, A.A., et al. (2021). Land-use change and rodent-borne diseases: hazards on the shared socioeconomic pathways. *Philosophical Transactions of The Royal Society B*, 376(1837), https://doi.org/https://doi.org/10.1098/rstb.2020.0362.

Gessner, U., Naeimi, V., Klein, I., Kuenzer, C., Klein, D., Dech, S. (2013). The relationship between precipitation anomalies and satellite-derived vegetation activity in central asia. *Global and Planetary Change*, 110: 74-87, https://doi.org/10.1016/j.gloplacha.2012.09.007.

Gimeno, L., Sorí, R., Vázquez, M., Stojanovic, M., Algarra, I., Eiras Barca, J., et al. (2022). Extreme precipitation events. *Wiley Interdisciplinary Reviews-Water*, 9(6), https://doi.org/10.1002/wat2.1611.

Gong, Z., Peng, D., Wen, J., Cai, Z., Wang, T., Hu, Y., et al. (2017). Research on trend of warm-humid climate in central asia. *Earth and Environmental Science*, 74: 12017, https://doi.org/10.1088/1755-1315/74/1/012017.

Guo, H., Bao, A., Chen, T., Zheng, G., Wang, Y., Jiang, L., et al. (2021). Assessment of cmip6 in simulating precipitation over arid central asia. *Atmospheric Research*, 252: 105451, https://doi.org/10.1016/j.atmosres.2021.105451.

Hamidov, A., Helming, K., Balla, D. (2016). Impact of agricultural land use in central asia: a review. *Agronomy for Sustainable Development*, 36(1), https://doi.org/10.1007/s13593-015-0337-7.

Hao, Z., Hao, F., Singh, V.P., Zhang, X. (2018). Changes in the severity of compound drought and hot extremes over global land areas. *Environmental Research Letters*, 13(12): 124022, https://doi.org/10.1088/1748-9326/aaee96.

Harris, I., Osborn, T.J., Jones, P., Lister, D. (2020). Version 4 of the cru ts monthly high-resolution gridded multivariate climate dataset. *Scientific Data*, 7(1), https://doi.org/10.1038/s41597-020-0453-3.

Hasegawa, T., Sakurai, G., Fujimori, S., Takahashi, K., Hijioka, Y., Masui, T. (2021). Extreme climate events increase risk of global food insecurity and adaptation needs. *Nature Food*, 2(8): 587-595, https://doi.org/10.1038/s43016-021-00335-4.

Hempel, S., Frieler, K., Warszawski, L., Schewe, J., Piontek, F. (2013). A trend-preserving bias correction – the isi-

mip approach. *Earth System Dynamics*, 4(2): 219-236, https://doi.org/10.5194/esd-4-219-2013.

Hu, Z., Li, Q., Chen, X., Teng, Z., Chen, C., Yin, G., et al. (2016). Climate changes in temperature and precipitation extremes in an alpine grassland of central asia. *Theoretical and Applied Climatology*, 126(3-4): 519-531, https://doi.org/10.1007/s00704-015-1568-x.

Huang, A., Zhou, Y., Zhang, Y., Huang, D., Zhao, Y., Wu, H. (2014). Changes of the annual precipitation over central asia in the twenty-first century projected by multimodels of cmip5. *Journal of Climate*, 27(17): 6627-6646, https://doi.org/10.1175/JCLI-D-14-00070.1.

Huang, X., Swain, D.L. (2022). Climate change is increasing the risk of a california megaflood. *Science Advances*, 8(32): q995, https://doi.org/10.1126/sciadv.abq0995.

Hurtt, G.C., Chini, L., Sahajpal, R., Frolking, S., Bodirsky, B.L., Calvin, K., et al. (2020). Harmonization of global land use change and management for the period 850 – 2100 (luh2) for cmip6. *Geoscientific Model Development*, 13(11): 5425-5464, https://doi.org/10.5194/gmd-13-5425-2020.

IPCC. (2021). Climate change 2021: the physical science basis contribution of working group i to the sixth assessment report of the intergovernmental panel on climate change.: Cambridge University Press.

Jiang, D., Sui, Y., Lang, X. (2016). Timing and associated climate change of a 2 °c global warming. *International Journal of Climatology*, 36(14): 4512-4522, https://doi.org/10.1002/joc.4647.

Jiang, J., Zhou, T., Chen, X., Zhang, L. (2020). Future changes in precipitation over central asia based on cmip6 projections. *Environmental Research Letters*(15): 54009, https://doi.org/https://doi.org/10.1088/1748-9326/ab7d03.

Jiang, J., Zhou, T. (2023). Agricultural drought over water-scarce central asia aggravated by internal climate variability. *Nature Geoscience*, 16(2): 154-161, https://doi.org/10.1038/s41561-022-01111-0.

Jiang, J., Zhou, T. (2021). Human - induced rainfall reduction in drought - prone northern central asia. *Geophysical Research Letters*, 48(7), https://doi.org/10.1029/2020GL092156.

Jones, B., O Neill, B.C., McDaniel, L., McGinnis, S., Mearns, L.O., Tebaldi, C. (2015). Future population exposure to us heat extremes. *Nature Climate Change*, 5(7): 652-655, https://doi.org/10.1038/nclimate2631.

Jong, B., Delworth, T.L., Cooke, W.F., Tseng, K., Murakami, H. (2023). Increases in extreme precipitation over the northeast united states using high-resolution climate model simulations. *Npj Climate and Atmospheric Science*, 18(6), https://doi.org/ https://doi.org/10.1038/s41612-023-00347-w.

Lau, W.K.M., Kim, K. (2012). The 2010 pakistan flood and russian heat wave: teleconnection of hydrometeorological extremes. *Journal of Hydrometeorology*, 13(1): 392-403, https://doi.org/10.1175/JHM-D-11-016.1.

Li, C., Zwiers, F., Zhang, X., Chen, G., Lu, J., Li, G., et al. (2019). Larger increases in more extreme local precipitation events as climate warms. *Geophysical Research Letters*, 46(12): 6885-6891, https://doi.org/10.1029/2019GL082908.

Li, C., Zwiers, F., Zhang, X., Li, G., Sun, Y., Wehner, M. (2021). Changes in annual extremes of daily temperature and precipitation in cmip6 models. *Journal of Climate*, 34(9): 3441-3460, https://doi.org/10.1175/JCLI-D-19-1013.1.

Li, L., Li, J., Yu, R. (2022). Evaluation of cmip6 highresmip models in simulating precipitation over central asia. *Advances in Climate Change Research*, 13(1): 1-13, https://doi.org/10.1016/j.accre.2021.09.009.

Li, Y., Guan, K., Schnitkey, G.D., DeLucia, E., Peng, B. (2019). Excessive rainfall leads to maize yield loss of a

783 comparable magnitude to extreme drought in the united states. *Global Change Biology*, 25(7): 2325-2337,
784 https://doi.org/10.1111/gcb.14628.

785 Li, Z., Li, Z., Yu, H., Song, L., Ma, J. (2019). Environmental significance and zonal characteristics of stable isotope
786 of atmospheric precipitation in arid central asia. *Atmospheric Research*, 227: 24-40,
787 https://doi.org/10.1016/j.atmosres.2019.04.022.

788 Liu, K., Wang, Q., Wang, M., Koks, E.E. (2023). Global transportation infrastructure exposure to the change of
789 precipitation in a warmer world. *Nature Communications*, 14(1), https://doi.org/10.1038/s41467-023-38203-3.

790 Liu, W., Sun, F., Feng, Y., Li, C., Chen, J., Sang, Y., et al. (2021). Increasing population exposure to global warm-
791 season concurrent dry and hot extremes under different warming levels. *Environmental Research Letters*, 16:
792 94002, https://doi.org/https://doi.org/10.1088/1748-9326/ac188f.

793 Liu, Y.R., Li, Y.P., Ma, Y., Huang, G.H., Zhou, X. (2022). Analyzing extreme precipitation and temperature in
794 central asia as well as quantifying their main and interactive effects under multiple uncertainties. *Journal of*
795 *Hydrology*, 607: 127469, https://doi.org/10.1016/j.jhydrol.2022.127469.

796 Liu, Z., Huang, J., Xiao, X., Tong, X. (2022). The capability of cmip6 models on seasonal precipitation extremes
797 over central asia. *Atmospheric Research*, 278: 106364, https://doi.org/10.1016/j.atmosres.2022.106364.

798 Liu, Z., Anderson, B., Yan, K., Dong, W., Liao, H., Shi, P. (2017). Global and regional changes in exposure to
799 extreme heat and the relative contributions of climate and population change. *Scientific Reports*, 7(1),
800 https://doi.org/10.1038/srep43909.

801 Ma, L., Hurtt, G.C., Chini, L.P., Sahajpal, R., Pongratz, J., Frolking, S., et al. (2020). Global rules for translating
802 land-use change (luh2) to land-cover change for cmip6 using glm2. *Geoscientific Model Development*, 13(7):
803 3203-3220, https://doi.org/10.5194/gmd-13-3203-2020.

804 Ma, Q., Zhang, J., Ma, Y., Game, A.T., Chen, Z., Chang, Y., et al. (2021). How do multiscale interactions affect
805 extreme precipitation in eastern central asia? *Journal of Climate*, 34(18): 7475-7491,
806 https://doi.org/10.1175/JCLI-D-20-0763.1.

807 Mariotti, A., Struglia, M.V., Zeng, N., Lau, K. (2002). The hydrological cycle in the mediterranean region and
808 implications for the water budget of the mediterranean sea. *Journal of Climate*, 15(13): 1674-1690,
809 https://doi.org/https://doi.org/10.1175/1520-0442(2002)015<1674:THCITM>2.0.CO;2.

810 Mondal, S.K., Wang, Y., Zhai, J., Su, B., Jiang, S., Huang, J., et al. (2022). Projected urban exposure to extreme
811 precipitation over south asia. *Science of the Total Environment*, 822: 153664,
812 https://doi.org/10.1016/j.scitotenv.2022.153664.

813 Murnane, R.J., Daniell, J.E., Schäfer, A.M., Ward, P.J., Winsemius, H.C., Simpson, A., et al. (2017). Future
814 scenarios for earthquake and flood risk in eastern europe and central asia. *Earth's Future*, 5(7): 693-714,
815 https://doi.org/10.1002/2016EF000481.

816 Ombadi, M., Risser, M.D., Rhoades, A.M., Varadharajan, C. (2023). A warming-induced reduction in snow fraction
817 amplifies rainfall extremes. *Nature*, https://doi.org/10.1038/s41586-023-06092-7.

818 Park, C.E., Jeong, S. (2022). Population exposure projections to intensified summer heat. *Earth's Future*, 10(2),
819 https://doi.org/10.1029/2021EF002602.

820 Peng, D., Zhou, T., Zhang, L., Zhang, W., Chen, X. (2020). Observationally constrained projection of the reduced
821 intensification of extreme climate events in central asia from 0.5 °c less global warming. *Climate Dynamics*, 54(1-
822 2): 543-560, https://doi.org/10.1007/s00382-019-05014-6.

823 Raymond, C., Horton, R.M., Zscheischler, J., Martius, O., AghaKouchak, A., Balch, J., et al. (2020). Understanding

and managing connected extreme events. *Nature Climate Change*, 10(7): 611-621, https://doi.org/10.1038/s41558-020-0790-4.

Samir, K., Wolfgang, L. (2017). The human core of the shared socioeconomic pathways: population scenarios by age, sex and level of education for all countries to 2100. *Global Environmental Change*, 42: 181-192, https://doi.org/10.1016/j.gloenvcha.2014.06.004.

Schiemann, R., Lüthi, D., Vidale, P.L., Schär, C. (2008). The precipitation climate of central asia—intercomparison of observational and numerical data sources in a remote semiarid region. *International Journal of Climatology*, 28(3): 295-314, https://doi.org/10.1002/joc.1532.

Scussolini, P., Aerts, J.C.J.H., Jongman, B., Bouwer, L.M., Winsemius, H.C., de Moel, H., et al. (2016). Flopros: an evolving global database of flood protection standards. *Natural Hazards and Earth System Sciences*, 16(5): 1049-1061, https://doi.org/10.5194/nhess-16-1049-2016.

Shi, X., Chen, J., Gu, L., Xu, C., Chen, H., Zhang, L. (2021). Impacts and socioeconomic exposures of global extreme precipitation events in 1.5 and 2.0 °c warmer climates. *Science of the Total Environment*, 766: 142665, https://doi.org/10.1016/j.scitotenv.2020.142665.

Sommer, R., Glazirina, M., Yuldashev, T., Otarov, A., Ibraeva, M., Martynova, L., et al. (2013). Impact of climate change on wheat productivity in central asia. *Agriculture, Ecosystems & Environment*, 178: 78-99, https://doi.org/10.1016/j.agee.2013.06.011.

Song, Y., Lv, M., Wang, M., Li, X., Qu, Y. (2021). Reconstruction of historical land surface albedo changes in china from 850 to 2015 using land use harmonization data and albedo look‐up maps. *Earth and Space Science*, 8(9), https://doi.org/10.1029/2021EA001799.

Su, B., Huang, J., Fischer, T., Wang, Y., Kundzewicz, Z.W., Zhai, J., et al. (2018). Drought losses in china might double between the 1.5 °c and 2.0 °c warming. *Proceedings of the National Academy of Sciences*, 115(42): 10600-10605, https://doi.org/10.1073/pnas.1802129115.

Sun, H., Wang, Y., Chen, J., Zhai, J., Jing, C., Zeng, X., et al. (2017). Exposure of population to droughts in the haihe river basin under global warming of 1.5 and 2.0 °c scenarios. *Quaternary International*, 453: 74-84, https://doi.org/10.1016/j.quaint.2017.05.005.

Sun, S., Dai, T., Wang, Z., Chou, J., Chao, Q., Shi, P. (2021). Projected increases in population exposure of daily climate extremes in eastern china by 2050. *Advances in Climate Change Research*, 12(6): 804-813, https://doi.org/10.1016/j.accre.2021.09.014.

Sun, X., Ge, F., Chen, Q., Fraedrich, K., Li, X. (2023). How striking is the intergenerational difference in exposure to compound heatwaves over southeast asia? *Earth's Future*, 11(6), https://doi.org/10.1029/2022EF003179.

Swain, D.L., Wing, O.E.J., Bates, P.D., Done, J.M., Johnson, K.A., Cameron, D.R. (2020). Increased flood exposure due to climate change and population growth in the united states. *Earth's Future*, 8(11), https://doi.org/10.1029/2020EF001778.

Swain, S., Hayhoe, K. (2015). Cmip5 projected changes in spring and summer drought and wet conditions over north america. *Climate Dynamics*, 44(9-10): 2737-2750, https://doi.org/10.1007/s00382-014-2255-9.

Tabari, H., Madani, K., Willems, P. (2020). The contribution of anthropogenic influence to more anomalous extreme precipitation in europe. *Environmental Research Letters*, 15(10): 104077, https://doi.org/10.1088/1748-9326/abb268.

Tandon, N.F., Zhang, X., Sobel, A.H. (2018). Understanding the dynamics of future changes in extreme precipitation intensity. *Geophysical Research Letters*, 45(6): 2870-2878, https://doi.org/10.1002/2017GL076361.

Taylor, K.E. (2001). Summarizing multiple aspects of model performance in a single diagram. *Journal of Geophysical Research. D. Atmospheres*, 106(D7): 7183-7192, https://doi.org/10.1029/2000JD900719.

Thackeray, C.W., Hall, A., Norris, J., Chen, D. (2022). Constraining the increased frequency of global precipitation extremes under warming. *Nature Climate Change*, 12(5): 441-448, https://doi.org/10.1038/s41558-022-01329-1.

Thomas, H.D., Brian, W., Reinette, B., Anne-Sophie, C., Carl, F., Eric F, L., et al. (2015). Synchronous failure: the emerging causal architecture of global crisis. *Ecology and Society*, 20(3), https://doi.org/10.5751/ES-07681-200306.

Tian, J., Zhang, Y. (2020). Detecting changes in irrigation water requirement in central asia under co2 fertilization and land use changes. *Journal of Hydrology*, 583: 124315, https://doi.org/10.1016/j.jhydrol.2019.124315.

Ullah, I., Saleem, F., Iyakaremye, V., Yin, J., Ma, X., Syed, S., et al. (2022). Projected changes in socioeconomic exposure to heatwaves in south asia under changing climate. *Earth's Future*, 10(2), https://doi.org/10.1029/2021EF002240.

Wang, A., Tao, H., Ding, G., Zhang, B., Huang, J., Wu, Q. (2023). Global cropland exposure to extreme compound drought heatwave events under future climate change. *Weather and Climate Extremes*, 40: 100559, https://doi.org/10.1016/j.wace.2023.100559.

Wang, J., Wang, H., Hong, Y. (2016). Comparison of satellite-estimated and model- forecasted rainfall data during a deadly debris-flow event in zhouqu, northwest china. *Atmospheric and Oceanic Science Letters*, 9(9): 139-145, https://doi.org/ https://doi.org/10.1080/16742834.2016.1142825.

Wang, Y. (2005). Observed trends in extreme precipitation events in china during 1961 – 2001 and the associated changes in large-scale circulation. *Geophysical Research Letters*, 32(9), https://doi.org/10.1029/2005GL022574.

Wang, Y., Wang, A., Zhai, J., Tao, H., Jiang, T., Su, B., et al. (2019). Tens of thousands additional deaths annually in cities of china between 1.5 °c and 2.0 °c warming. *Nature Communications*, 10(1), https://doi.org/10.1038/s41467-019-11283-w.

Warszawski, L., Frieler, K., Huber, V., Piontek, F., Serdeczny, O., Schewe, J. (2014). The inter-sectoral impact model intercomparison project (isi – mip): project framework. *Proceedings of the National Academy of Sciences*, 111(9): 3228-3232, https://doi.org/10.1073/pnas.1312330110.

Watts, N., Amann, M., Arnell, N., Ayeb-Karlsson, S., Beagley, J., Belesova, K., et al. (2021). The 2020 report of the lancet countdown on health and climate change: responding to converging crises. *The Lancet*, 397(10269): 129-170, https://doi.org/https://doi.org/10.1016/S0140-6736(20)32290-X.

Wei, W., Zou, S., Duan, W., Chen, Y., Li, S., Zhou, Y. (2023). Spatiotemporal variability in extreme precipitation and associated large-scale climate mechanisms in central asia from 1950 to 2019. *Journal of Hydrology*, 620: 129417, https://doi.org/10.1016/j.jhydrol.2023.129417.

Wen, S., Wang, A., Tao, H., Malik, K., Huang, J., Zhai, J., et al. (2019). Population exposed to drought under the 1.5 °c and 2.0 °c warming in the indus river basin. *Atmospheric Research*, 218: 296-305, https://doi.org/10.1016/j.atmosres.2018.12.003.

Xie, T., Huang, W., Chang, S., Zheng, F., Chen, J., Chen, J., et al. (2021). Moisture sources of extreme precipitation events in arid central asia and their relationship with atmospheric circulation. *International Journal of Climatology*, 41(S1), https://doi.org/10.1002/joc.6683.

Xu, C., Li, J., Zhao, J., Gao, S., Chen, Y. (2015). Climate variations in northern xinjiang of china over the past 50 years under global warming. *Quaternary International*, 358: 83-92, https://doi.org/10.1016/j.quaint.2014.10.025.

Xu, P., Wang, L., Ming, J. (2022). Central asian precipitation extremes affected by an intraseasonal planetary wave

pattern. *Journal of Climate*, 35(8): 2603-2616, https://doi.org/10.1175/JCLI-D-21-0657.1.

Xue, T., Tang, G., Sun, L., Wu, Y., Liu, Y., Dou, Y. (2017). Long-term trends in precipitation and precipitation extremes and underlying mechanisms in the u.s. Great basin during 1951-2013. *Journal of Geophysical Research: Atmospheres*, 122(12): 6152-6169, https://doi.org/10.1002/2017JD026682.

Yang, Y., Jin, C., Ali, S. (2020). Projection of heat wave in china under global warming targets of 1.5 °c and 2 °c by the isimip models. *Atmospheric Research*, 244: 105057, https://doi.org/10.1016/j.atmosres.2020.105057.

Yao, J., Chen, Y., Chen, J., Zhao, Y., Tuoliewubieke, D., Li, J., et al. (2021). Intensification of extreme precipitation in arid central asia. *Journal of Hydrology*, 598: 125760, https://doi.org/10.1016/j.jhydrol.2020.125760.

Yu, X., Zhao, Y., Ma, X., Yao, J., Li, H. (2018). Projected changes in the annual cycle of precipitation over central asia by cmip5 models. *International Journal of Climatology*, 38(15): 5589-5604, https://doi.org/10.1002/joc.5765.

Yuan, X., Wang, W., Cui, J., Meng, F., Kurban, A., De Maeyer, P. (2017). Vegetation changes and land surface feedbacks drive shifts in local temperatures over central asia. *Scientific Reports*, 7(1), https://doi.org/10.1038/s41598-017-03432-2.

Yue, Y., Yan, D., Yue, Q., Ji, G., Wang, Z. (2021). Future changes in precipitation and temperature over the yangtze river basin in china based on cmip6 gcms. *Atmospheric Research*, 264: 105828, https://doi.org/10.1016/j.atmosres.2021.105828.

Zhang, G., Wang, H., Gan, T.Y., Zhang, S., Shi, L., Zhao, J., et al. (2022). Climate change determines future population exposure to summertime compound dry and hot events. *Earth's Future*, 10(11), https://doi.org/10.1029/2022EF003015.

Zhang, J., Wang, F. (2019). Changes in the risk of extreme climate events over east asia at different global warming levels. *Water*, 11(12): 2535, https://doi.org/10.3390/w11122535.

Zhang, J., Ma, Q., Chen, H., Zhao, S., Chen, Z. (2021). Increasing warm-season precipitation in asian drylands and response to reducing spring snow cover over the tibetan plateau. *Journal of Climate*: 1-69, https://doi.org/10.1175/JCLI-D-20-0479.1.

Zhang, J., Wang, F. (2022). Future changes in extreme precipitation in central asia with 1.5 – 4°c global warming based on coupled model intercomparison project phase 6 simulations. *International Journal of Climatology*, 42(16): 8509-8525, https://doi.org/10.1002/joc.7740.

Zhang, L., Chen, X.Q., Liu, S., Zhang, Q., Zhao, J., Dai, J.Y., et al. (2018). Space-time-coding digital metasurfaces. *Nature Communications*, 9(1), https://doi.org/10.1038/s41467-018-06802-0.

Zhang, M., Chen, Y., Shen, Y., Li, Y. (2017). Changes of precipitation extremes in arid central asia. *Quaternary International*, 436: 16-27, https://doi.org/10.1016/j.quaint.2016.12.024.

Zhang, M., Yu, H., King, A.D., Wei, Y., Huang, J., Ren, Y. (2020). Greater probability of extreme precipitation under 1.5 °c and 2 °c warming limits over east-central asia. *Climatic Change*, 162(2): 603-619, https://doi.org/10.1007/s10584-020-02725-2.

Zhang, M., Chen, Y., Shen, Y., Li, B. (2019). Tracking climate change in central asia through temperature and precipitation extremes. *Journal of Geographical Sciences*, 29(1): 3-28, https://doi.org/10.1007/s11442-019-1581-6.

Zhang, W., Furtado, K., Wu, P., Zhou, T., Chadwick, R., Marzin, C., et al. (2021). Increasing precipitation variability on daily-to-multiyear time scales in a warmer world. *Science Advances*, 7(31), https://doi.org/10.1126/sciadv.abf8021.

946 Zhang, W., Zhou, T. (2020). Increasing impacts from extreme precipitation on population over china with global
947 warming. *Science Bulletin*, 65(3): 243-252, https://doi.org/10.1016/j.scib.2019.12.002.

948 Zhao, Y., Yu, X., Yao, J., Dong, X. (2018). Evaluation of the subtropical westerly jet and its effects on the projected
949 summer rainfall over central asia using multi-cmip5 models. *International Journal of Climatology*, 38: e1176-
950 e1189, https://doi.org/10.1002/joc.5443.

951 Zhou, S., Yu, B., Zhang, Y. (2023). Global concurrent climate extremes exacerbated by anthropogenic climate
952 change. *Science Advances*, 9(10): o1638, https://doi.org/10.1126/sciadv.abo1638.

953 Zou, S., Abuduwaili, J., Duan, W., Ding, J., De Maeyer, P., Van De Voorde, T., et al. (2021). Attribution of changes
954 in the trend and temporal non-uniformity of extreme precipitation events in central asia. *Scientific Reports*, 11(1),
955 https://doi.org/10.1038/s41598-021-94486-w.

956 Zscheischler, J., Martius, O., Westra, S., Bevacqua, E., Raymond, C., Horton, R.M., et al. (2020). A typology of
957 compound weather and climate events. *Nature reviews. Earth & environment*, 1(7): 333-347,
958 https://doi.org/10.1038/s43017-020-0060-z.

959